

Measurement of the Prompt Neutrons Emitted in the Fission of ^{209}Bi and ^{238}U Induced by 155-MeV Protons

E. Cheifetz, and Z. Fraenkel

Department of Nuclear Physics, Weizmann Institute of Science, Rehovot, Israel

and

J. Galin, M. Lefort, J. Péter, and X. Tarrago

Laboratoire Chimie Nucléaire, Institut Physique Nucléaire, Orsay, France

(Received 10 February 1970)

The energy distribution of the neutrons emitted in the fission of ^{209}Bi and ^{238}U induced by 155-MeV protons was measured at 0 and 90° with respect to the fission fragment direction. The neutron velocity was measured by the time-of-flight method in coincidence with the measurement of the kinetic energy of the two fission fragments. The number of postfission neutrons as a function of the fragment mass and the energy distribution of the postfission neutrons were determined without reference to any theoretical model. The number of prefission neutrons was determined on the assumption of isotropic emission from the excited nucleus. With this assumption we find that 5.8 ± 1.0 prefission neutrons are emitted from U and 6.9 ± 1.0 from Bi. The number of postfission neutrons is 5.1 ± 0.5 for U and 4.2 ± 0.5 for Bi. We compare our experimental results with the results of calculations based on the usual model of a prompt intranuclear cascade followed by neutron evaporation-fission competition with several assumptions for Γ_f/Γ_n (ratio of fission width to neutron emission width). We are unable to find a consistent set of parameters which would give good agreement between the calculated results, our experimental results, radiochemical results for spallation residues, and total fission cross-section measurements. Our experimental results indicate that Γ_f/Γ_n decreases at high excitation energies. We find that the number of postfission neutrons increases rapidly with increasing fragment mass for both Bi and U. When our results for U are compared with low-energy fission data for this element, it is found that almost all the additional excitation energy available in high-energy fission is concentrated in the heavy fragment.

I. INTRODUCTION

When fission is induced in heavy nuclei by high energy ($\gtrsim 100$ MeV) protons, emission of neutrons may occur in any of the three stages of the reaction: (1) neutron emission in the fast intranuclear cascade process, (2) neutron evaporation from the excited nucleus before fission occurs, and (3) neutron evaporation from the excited fission fragments.

The emission of neutrons in the fast intranuclear cascade process is not believed to be related to the subsequent fission process, and hence it will not be discussed here in any detail. Experimentally, these neutrons are characterized by the sharp forward peaking of their angular distribution and by their high kinetic energies. By confining the neutron measurement to a plane perpendicular to the beam direction and to neutrons of kinetic energy below 10 MeV, the probability of their detection is greatly reduced. Yet the fast-cascade neutrons cannot be completely ignored, even under these experimental conditions.

The investigation of the second and third groups of neutrons (prefission evaporation neutrons and postfission neutrons) is of great importance to the understanding of the fission process for two rather

different reasons: The number of *prefission* neutrons is directly related to the competition between neutron emission and fission at high excitation energies. From the number of prefission neutrons for several bombarding energies and target nuclei one can determine $\Gamma_f/\Gamma_n(E^*, A_0)$, the ratio of the fission width to the neutron emission width, i.e., the probability of fission relative to that of neutron emission as a function of excitation energy and mass of the fissioning nucleus. The measurement of the number and kinetic energy spectrum of the *postfission* neutrons as a function of the fragment mass and the total kinetic energy of the two fragments determines the total excitation energy in high-energy fission and its division between the two fragments. It is of particular interest to compare such measurements for U with the results of low-energy fission, and thereby obtain additional insight into the differences between the low- and high-energy fission processes.

The experimental separation of prefission and postfission neutrons requires the measurement of the energy and angular distribution (with respect to the direction of the fission fragments) of the neutrons, as well as the measurement of the kinetic energy of the two fragments. It also requires

an assumption concerning the angular distribution of the neutrons emitted from the fragments. (Normally this angular distribution is assumed to be isotropic in the c.m. system of the fragments.)

Harding and Farley¹ were the first to try to determine by this method the number of prefission and postfission neutrons in high-energy fission. They measured the number of neutrons at 0 and 90° with respect to the direction of the fission fragments for the fission of ²³⁸U bombarded by 147-MeV protons. They found that the ratio of the number of neutrons at 0° to the number of neutrons at 90° with respect to the fission fragment direction was $N(0^\circ)/N(90^\circ) = 1.27 \pm 0.11$. The total number of neutrons was previously measured by Harding,² who obtained 13.1 ± 1.8 . The experiment of Harding and Farley suffered from poor statistics and a very high random rate. They could not measure the neutron energies, and hence had to assume that the efficiency of their neutron detector (a methane proportional counter) was the same for the neutron spectra at 0 and 90° despite the difference between the two spectra.

The relative probabilities of fission and neutron emission Γ_f/Γ_n can also be determined by radiochemical measurements. The method consists of measuring, radiochemically, the reaction yield of the nuclides near the target nucleus, thereby determining the cross section for the reaction which did *not* involve fission throughout all stages of the deexcitation process. The experimental results are compared with the calculations of the fast intranuclear cascade process followed by the deexcitation of the nucleus through successive evaporation of neutrons or fission (which may occur at any stage of the neutron evaporation process). Studies of this kind were made by Lindner and Turkevich³ for the data of Lindner and Osborn⁴ (340-MeV protons on ²³²Th and ²³⁸U); by Lefort, Simonoff and Tarrago⁵ for 82- and 150-MeV protons on ²³²Th; by Pate and Poskanzer⁶ for 680-MeV and 1.8-GeV protons on ²³²Th, ²³⁵U, and ²³⁸U; and by Le Beyec and Lefort⁷ for 20-156-MeV protons on ²⁰⁹Bi.

In the following, we describe an experiment in which we measured the energy and angular distribution of the neutrons accompanying fission of ²⁰⁹Bi and ²³⁸U nuclei bombarded with 155-MeV protons from the Orsay synchrocyclotron. The energy and angle (with respect to the fission fragment direction) of the neutron, as well as the kinetic energy of the two fission fragments, were measured with the aid of an on-line computer and stored event by event on magnetic tape. The tapes were later analyzed with an off-line computer. The measurement of the kinetic energy and direction of the neutron and the two fission fragments

makes it possible to obtain the number and the energy spectrum of the prefission neutrons, as well as the number and the energy spectrum of the neutrons emitted from each of the fission fragments. The latter were determined as a function of the fragment mass and total kinetic energy. In the present paper we shall briefly discuss the comparison of our experimental results with calculations of the fast intranuclear cascade, and the subsequent deexcitation of the nucleus by neutron evaporation and fission.

We discuss in Sec. II the experimental arrangement. The analysis of the experimental results is explained in Sec. III. We present our experimental results in Sec. IV, and these results are discussed in Sec. V. We summarize our conclusions in Sec. VI.

II. EXPERIMENTAL ARRANGEMENT

A. Brief Description of the Experimental Method

The purpose of the experiment was to measure the energy and angular distributions of the neutrons emitted from the target nucleus before it underwent fission (more precisely before the fission fragments began their motion), and the number of neutrons emitted from the moving fragments. The neutrons were measured at several angles with respect to the fission fragments. But all measurements were performed at the same angle with respect to the beam direction, so as to eliminate corrections due to angular momentum imparted by the bombarding particle to the fissioning system. The energies of the two fission fragments were measured with solid-state detectors, and the neutron velocities were measured by the time-of-flight method. The start pulse was given by one of the fission fragment detectors and the stop pulse by the neutron detector. This detector was a plastic scintillator which was outside the vacuum chamber. Pure random events in the time-of-flight spectrum were measured simultaneously (but stored separately) with the "true" spectrum which contained both the true as well as random events. This enabled random subtraction independent of the changes in the beam profile, beam intensity, target thickness, etc.

The fragment energies and neutron velocity were stored in chronological order by an on-line computer on magnetic tape. The tapes were later analyzed with the aid of a large off-line computer. The fragment masses and total kinetic energy were obtained from the fragment energies. The neutron energies were obtained from the time-of-flight data after correction for the time interval

between the true moment of fission and the "start" time of the time-of-flight system (this difference is equal to the flight time of the fission fragment). The detection efficiency of the neutron detector was obtained by measuring the neutron spectrum for the spontaneous fission of ^{252}Cf , and comparing our results with the accurate measurements of Bowman *et al.*⁸ The neutrons were measured in the energy interval 0.5–9.0 MeV, which includes almost the whole spectrum of interest.

B. Geometrical Arrangement

In order to increase the counting rate, two neutron detectors and two pairs of fission fragment detectors were used. The two neutron detectors were placed at 90° to each other in a plane perpendicular to the beam and at a distance of 35 cm from the center of the target (which was also in the same plane). The two pairs of fission fragment detectors were also placed at 90° to each other at 10 cm from the center of the target (Fig. 1). One detector of each pair was colinear with one of the neutron detectors in the target-neutron detector plane. The second detector of each fission fragment detector pair was placed in the forward hemisphere at 4° (for ^{238}U) or 7° (for ^{209}Bi) with

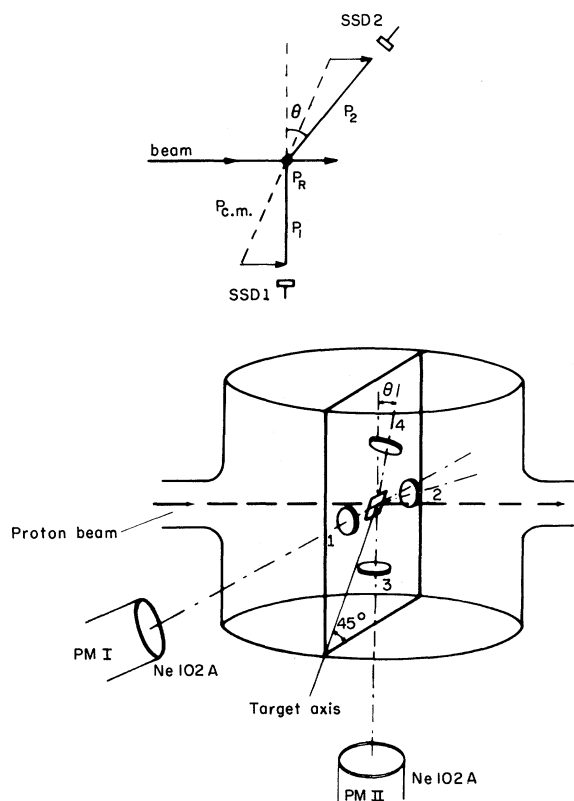


FIG. 1. The geometrical arrangement of the experiment.

respect to the neutron detector-target plane. The purpose of the forward angle of one of the detectors is to correct for the recoil momentum imparted to the nucleus by the bombarding particle. Kowalski and Stephan⁹ found that the mean value for the recoil angle was 4° for $^{238}\text{U} + 155\text{-MeV } p$ and 7° for $^{209}\text{Bi} + 155\text{-MeV } p$. However, since the width of the recoil-angle distribution¹⁰ was of the same order of magnitude as the acceptance angle of our detectors, our choice of the detector angle introduces a certain bias against very small and very large recoil momenta. This is discussed in greater detail in Appendix A.

C. Target Chamber

The target chamber was made of aluminium with a thickness of 0.7 cm. Its shape was that of a cylinder of 66-cm diam with dome-shaped top and bottom covers. The distance between the centers of the top and bottom covers was 60 cm. Thus the chamber resembled roughly a spherical shell of 0.7-cm thickness and ~ 60 -cm diam. The axis of the target holder was at 45° to the horizontal detectors, and in the detector plane (normal to the beam direction). The correct target angle was obtained by rotating the target by 45° with respect to the detector plane. Thus the effective thickness of the target, as seen by both the beam and the detectors, was twice its actual thickness.

D. Fission Fragment Detectors

The fission fragments were detected with surface-barrier detectors. One detector in each pair had an active area of 4 cm^2 , and the other had an active area of 3 cm^2 . The experimental coincidence efficiency for each pair of detectors (defined as the ratio of the coincidence rate to the singles rate in the smaller detector) was approximately 50%. This relatively low number was mainly due to the finite size of the beam spot, but was also due to the spread of the recoil momentum of the target nucleus and the spread in the fragment direction due to neutron emission. (See Appendix A.) The detectors were covered with $40\text{-}\mu\text{g}/\text{cm}^2$ Ni foils as a protection against low-energy radiation.

The detector performance was checked before, during, and after the experimental runs by observing the energy spectra of a ^{252}Cf source. Each of the detectors received a total dose of $\sim 3 \times 10^7$ fission fragments. Although a small change in the detector gain was observed (and corrected for) during the experimental runs, no detectable change occurred in the shape of the ^{252}Cf spectra.

E. Neutron Detectors

The neutrons were detected by NE102A plastic scintillators¹¹ of 11-cm diam and 2.5-cm thick-

ness. The scintillators were mounted on 58 AVP photomultipliers. The pulse from the anode was fed directly to a fast discriminator which generated the "stop" pulse of the time-to-amplitude converter. This discriminator was calibrated with the aid of γ rays from ^{137}Cs , ^{22}Na , and ^{133}Ba sources. The discriminator threshold was set at a γ -ray energy of 50–90 keV, which corresponds to a proton energy of 300–600 keV.¹² This value of the discriminator threshold was obtained by requiring a singles count rate of the detectors of not more than $(1-2) \times 10^4/\text{sec}$ with the beam on. (The instantaneous rate was actually higher by a factor of 10–20 due to the beam duty cycle of 5–10%.) The dc current in the voltage divider of the photomultiplier base was approximately 8 mA, and this rendered negligible the effect of the counting rate on the photomultiplier gain.

The detection efficiency of the scintillator as a function of the neutron energy was obtained by comparing the time-of-flight spectra obtained for ^{252}Cf with the results of Bowman *et al.*³ This will be discussed in greater detail in the next chapter.

F. Proton Beam and Targets

The proton beam of the Orsay synchrocyclotron has an energy of 155 ± 3 MeV and the high-frequency structure of the form of the positive part of a 20-MHz sine wave. The low-frequency FM

period is 2200 μsec . When operating in the "stochastic" mode the duty cycle is 5–10%. The beam had a cross section of approximately 1 cm^2 with a considerable halo around it. However, the target frame was made large enough to render negligible the γ background due to protons hitting the frame. The U, and Bi targets were prepared by evaporating natural U, in the form of UF_4 and metallic Bi on a backing of $40\text{-}\mu\text{g}/\text{cm}^2$ cellulose acetate. Several target thicknesses were used so as to check the effect of the target thickness. They were in the range of 80–150 $\mu\text{g}/\text{cm}^2$ (actual thickness).

G. Electronic System

The signal from the solid-state detectors was fed to time pick-off units and to charge-sensitive pre-amplifiers, Figure 1. The time pick-off units fed timing pulses to fast discriminators, which in turn produced logic pulses of two lengths for the fast-coincidence circuits. The discriminators of the two detectors, which gave the "start" signal for the time-to-amplitude converters (TAC) for the neutron time-of-flight measurement, produced logic pulses of 100 nsec. The anode signal of each photomultiplier (PM) was fed to a fast discriminator which produced a logic pulse of 100 nsec, which served as the "stop" pulse of the TAC. The TAC consisted of a logic AND circuit and integrator. The amplitude of the TAC output pulse was

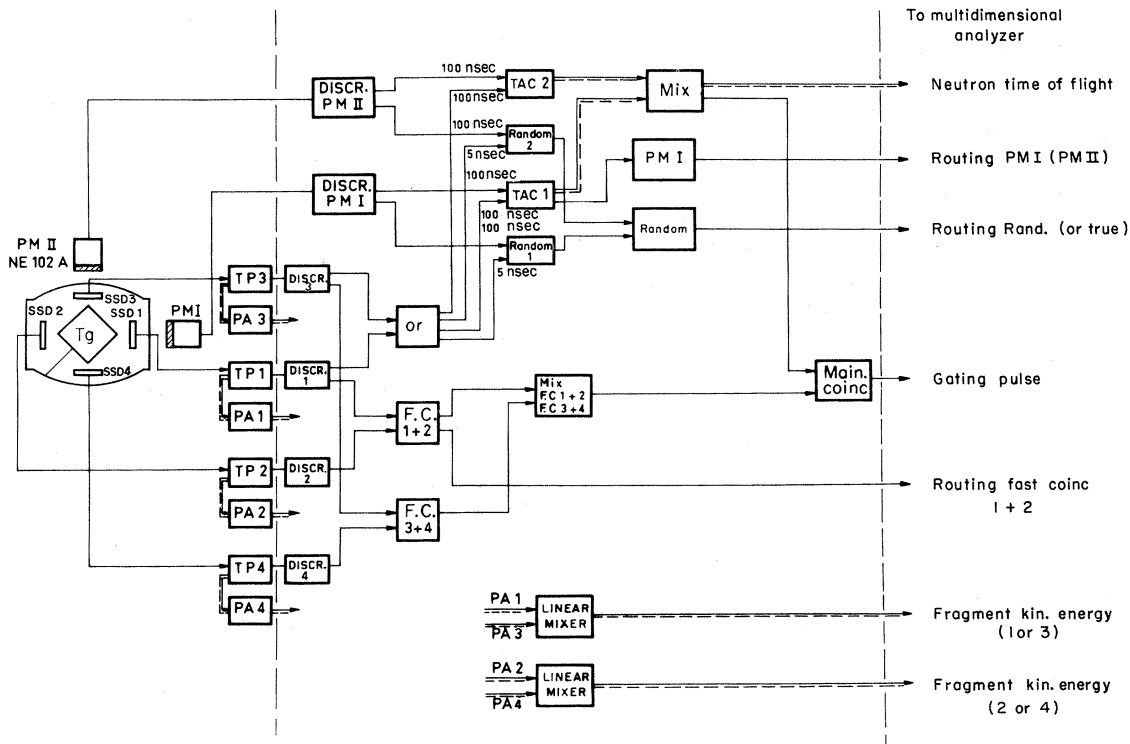


FIG. 2. The electronics block diagram of the experiment.

proportional to the time overlap of the "start" and "stop" pulses, and thus measured the time of flight of the neutron. A second AND circuit served as an indicator of random events. The "start" pulse from the solid-state detector (SSD) was clipped to a length of 5 nsec, and fed into the AND circuit together with the 100-nsec "stop" pulse from the photomultiplier. An overlap between the photomultiplier pulse and the clipped SSD pulse (which was somewhat delayed) indicated that the "stop" pulse had arrived before the "start" pulse, and hence the event was classified as a random event.

The time structure of the random events was correlated with the time structure of the beam to the extent that these events were due to prompt γ rays from the interaction of the beam with the distinct objects such as the target, the backing, the slits, the Faraday cup, etc. Random events which were a mirror image of this time structure also existed in the "true" time-of-flight data due to random events which came in the correct order, i.e., "start" before "stop". These could therefore be correctly subtracted from the true events.

Fast signals from the time-pick-off units of the two detectors in each pair of fission detectors were brought to a fast-coincidence unit. The output signal from this coincidence units, as well as a logic signal from the TAC, were fed into the slow (MAIN) coincidence circuit which produced the gate signal for the analog-to-digital convertors (ADC) and the on-line computer.

The experimental arrangement consisted of two neutron detectors and two pairs of fission detectors. Thus, in addition to three analog signals (the output of one TAC and two solid-state detectors), three logic signals were fed into the computer in order to fully identify each event, one determining which of the two neutron detectors detected the neutron (or γ), the second determining which of the two pairs of solid-state detectors detected the two fission fragments, and the third to signify whether the event was a "true" (correct order of TAC input signals) or random (reversed order) event.

H. ADC's and On-Line Computer

The three ADC's were of the successive approximation type and each had 100 channels. The analog portion of the events was thus described by a six-digit decimal number. An additional digit coded the three logic signals, and the eighth digit characterized the type of experiment (U, californium calibration, or pulser events). The eight-digit numbers were stored successively in a 23-word buffer memory. When the buffer was full, its con-

tent was transferred to the memory of the IBM 1610 on-line computer. Here they were transferred to an IBM-compatible tape in records of 253 events each. In addition, the events were sorted into 12 single-dimensional spectra: four fission fragment spectra, four "true" time-of-flight spectra corresponding to the four possible combinations of detectors in a given event, and four random time-of-flight spectra. The mean values of the fission fragment energy spectra were calculated and printed out every 100 records (25.3×10^3 events). This procedure made possible a continuous check of the gain stability of the solid-state detectors.

III. ANALYSIS OF THE EXPERIMENTAL RESULTS

A. Fission Fragment Kinetic Energies and Masses

We have used the calibration procedure of Schmitt, Kiker, and Williams¹³ to obtain the kinetic energy E_i of fragment i in terms of its mass A_i and pulse height X_i .

$$E_i = (a + a'A_i)X_i + b + b'A_i, \quad (1)$$

where a , a' , b , b' are constants determined by the positions of the light and heavy peaks P_L and P_H of the ²⁵²Cf fission spectrum measured under identical experimental conditions. E_i and A_i are obtained by an iteration procedure. It is based on the assumption that $A_0 = A_1 + A_2$, the mass of the fissioning nucleus is known for each event. A_0 is determined by the number of particles emitted before fission. In the present experiment we measured the *average* number of neutrons evaporated before fission. In addition to these, there are particles emitted in the fast-intranuclear-cascade process preceding the neutron evaporation stage. The number of these particles was not measured in the present experiment. The calculation of the intranuclear-cascade process¹⁴ shows that average number of particles emitted in this process is approximately 1.5 for both Bi and U targets bombarded with 155-MeV protons. The experimental results of the present investigation are that the average number of pre-fission evaporation neutrons is 5.8 ± 1.0 for U and 6.9 ± 1.0 for Bi. Thus the average total number of particles emitted prior to fission is 7.3 ± 1.0 for U and 8.4 ± 1.0 for Bi. (To be exact, the average number of fast-cascade nucleons should be determined from the cascades which subsequently undergo fission rather than from all cascades.) However, since the assumption of a fixed value for A_0 is only an

approximation, we assumed arbitrarily for the purpose of calculating the kinetic energy of the two fragments that the mass of the fissioning nucleus is $A_0 = 205$ in the case of the Bi target, and $A_0 = 234$ for U (i.e., the total number of nucleons emitted before fission is 5 for both Bi and U). It should however be emphasized that E_1 and E_2 are mainly dependent on the mass *ratio*, which was measured directly for each event in our experiment. E_1 and E_2 depend only to second order on our assumed value for A_0 , and thus the error introduced in the values for E_1 by our procedure is negligible. The details of the calculation are given in Appendix B.

B. Neutron Spectrum

1. Zero-Time Correction

The pulse initiating the neutron time-of-flight measurement was produced by one of the fragments hitting solid-state detector I or III (see Fig. 2). The measured neutron time of flight must therefore be corrected for the flight time of this fission fragment. This correction was made off line. The velocity of the fragment was calculated from its kinetic energy and mass (see preceding paragraph). This correction was made separately for each event. The correction reduced the width of the experimental γ peak from about 4 nsec to 3 nsec full width at half maximum (FWHM).

2. Random- and γ -Peak Subtraction

The experimentally measured spectrum of random events was used to subtract the contribution of random events to the neutron time-of-flight spectrum. The random events are partly correlated in time with the beam pulse structure (e.g., random events due to γ rays emitted from the backing), and partly uncorrelated to the beam pulse structure (e.g. random events due to the neutrons which were emitted with a wide velocity distribution from remote objects such as the beam catcher). The beam pulse structure had the form of the positive part on a sine wave with a period of 50 nsec. The random spectrum was therefore fitted by a least-squares method to a function consisting of a constant term plus a sine-wave term of a period of 50 nsec (the addition of a \sin^2 term did not improve the fit substantially). The fitted random spectrum thus obtained was subtracted from the neutron time-of-flight spectrum.

The time-of-flight spectrum obtained after random subtraction at 0 and 90° with respect to the fission fragment direction is shown in Fig. 3, together with the random spectrum. It is seen that

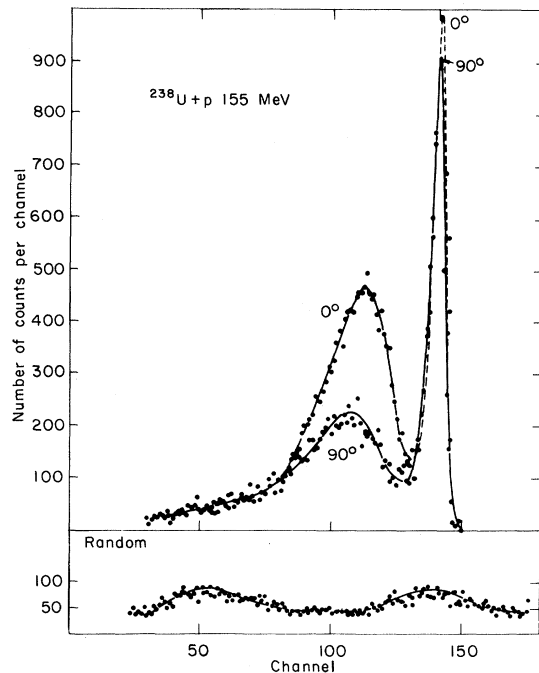


FIG. 3. The neutron time-of-flight spectrum at 0 and 90° to the fragment direction for U + 155-MeV p. The random spectrum has been subtracted from the time-of-flight spectra. The random spectrum at 0° is shown separately.

the γ peak (the sharp peak in the time-of-flight spectrum) coincides in time with the maximum in the random spectrum, indicating that the time structure in the random spectrum is mainly due to γ rays emitted in the target and backing or their immediate vicinity.

In order to obtain the true neutron velocity spectrum, the γ peak must be subtracted from the time-of-flight spectrum. This subtraction is somewhat uncertain because of the fact that there is a certain amount of overlap between the γ peak and the highest neutron velocities of the time-of-flight spectrum. It was therefore assumed that the *shape* of the true γ peak is given by the shape of this peak in the time-of-flight spectrum for ^{252}Cf at 90° to the direction of the fission fragments. (In this spectrum there are relatively few neutrons and no background due to random events.)

C. Correction for Dispersion in the Measurement of the Neutron Velocity

The dispersion in the measurement of the neutron velocity has two main causes: (1) the inherent time resolution of the system, i.e., the uncertainty in the flight *time*; (2) the uncertainty of the exact position of the interaction of the neutron in the scintillator, i.e. the uncertainty in the length

of the flight *path*. The time resolution of the electronic system is indicated by the width of the γ peak (the error due to the uncertainty in the flight distance is negligible in the case of γ rays). The standard deviation of the time resolution curve is therefore $\sigma_t = 1.3$ nsec (the standard deviation of the γ peak). The uncertainty of the flight distance and its standard deviation σ_D for every neutron velocity may be calculated by assuming the detection efficiency of the scintillator to be given by the single-scattering probability in the hydrogenic fraction of the scintillator (see Bowman *et al.*⁸ for details). The variance of the neutron velocity dispersion σ_v^2 is therefore given by

$$\sigma_v^2/v^2 = \sigma_D^2/\bar{D}^2 + \sigma_t^2/t^2, \quad (2)$$

where \bar{D} is the average flight distance of the neutrons, t is the flight time of the neutron, and $v = \bar{D}/t$ is the velocity of the neutron. In correcting the time-of-flight spectrum for the velocity dispersion, a procedure based on a suggestion by Terrell¹⁵ was followed: The neutron peak in the time-of-flight spectrum (see left peak in Fig. 3) is divided into two parts, one to the left and the other one to the right of the most probable value X_0 , and each part is assumed to have the shape of half a Gaussian distribution with standard deviation σ_l and σ_r , respectively. The correction consists of shifting each experimental value X of the time-of-flight distribution to a new value $X + \Delta X$, where

$$\Delta X = (X_0 - X)(\sigma_v^2/\sigma_t^2)(t^4 s^4/\bar{D}^2), \quad (3)$$

where $\sigma_l = \sigma_t$ for $X < X_0$, and $\sigma_r = \sigma_t$ for $X > X_0$. X and σ_t are given in terms of the number of channels. (Note that X increases as the time of flight decreases.) s is the channel width in units of time. The effect of shifting $X \rightarrow X + \Delta X$ is to shift the experimental points towards the most probable value X_0 thus reducing the width of the neutron-flight-time distribution.

D. Neutron-Detector Efficiency

The efficiency of the neutron detectors was determined by replacing the target with a ²⁵²Cf source and comparing the measured time-of-flight spectrum at 0, 30, 60, and 90° with respect to the fragment direction with results of Bowman *et al.*⁸ Zero-time correction, random event and γ -peak subtraction (there is, of course, no time structure in the random distribution for ²⁵²Cf), and dispersion correction were performed in the manner described above. Bowman *et al.*⁸ mea-

sured the neutron spectrum at 11.25, 22.50, 33.75, 45.00, 56.25, 67.50, 78.75, and 90.00° with respect to the direction of the light and the heavy fragments for 31 neutron velocities in the range of 1.0–4.4 cm/nsec. Their tabulated results were transformed to the angles of our experiment by fitting their angular distribution for each neutron velocity value to a third-order Legendre polynomial. Their angular distributions were also dispersed in order to match the finite size of our detectors. The efficiency $\epsilon(v, \theta)$ for each velocity value and each experimental angle with respect to the fission fragment direction was obtained by the equation⁸

$$\epsilon(v, \theta) = N\bar{D}/[\rho(v, \theta)v^4\omega sR], \quad (4)$$

where N is the number of counts in the time-of-flight channel (after all corrections have been made), $\rho(v, \theta)$ is the neutron velocity density as given by Bowman *et al.*,⁸ ω is the solid angle subtended by the neutron detector, and R is the total number of fission coincidences (uncorrelated with neutrons) measured by the fission fragment detectors.

The efficiency $\epsilon(v, \theta)$ obtained in the above manner is an *effective efficiency* which includes the effects of neutron absorption and scattering and $(n, n'\gamma)$ reactions in the walls of the target chamber and its vicinity. These effects are the reason that the efficiency is angle dependent, and that a different value for $\epsilon(v)$ is obtained for 0 and 90° with respect to the direction of the fission fragments. When the neutron angular and energy distributions in the ²⁰⁹Bi and ²³⁸U experiments are calculated on the basis of this effective efficiency function, the results are already corrected for scattering and $(n, n'\gamma)$ contribution, assuming that the shape of the angular and energy distributions of the neutrons is the same for ²⁵²Cf spontaneous fission and for the fission of ²⁰⁹Bi and ²³⁸U bombarded by 155-MeV protons. Since this is not the case, some corrections must be made. This matter is discussed in greater detail in Appendix C. There we also present theoretical estimates of the scattering corrections.

For most of the analysis, we used the neutron-detection efficiency function $\epsilon(\theta, v)$ obtained in the above manner. In addition an "uncorrected" efficiency function $\epsilon'(\theta, v)$ was calculated. This function differed from the "corrected" function $\epsilon(\theta, v)$ in that it was calculated on the basis of the time-of-flight data for ²⁵²Cf which were not corrected for dispersion (see Sec. III C above). The "uncorrected" efficiency function was used to calculate the number of neutrons in the cases where

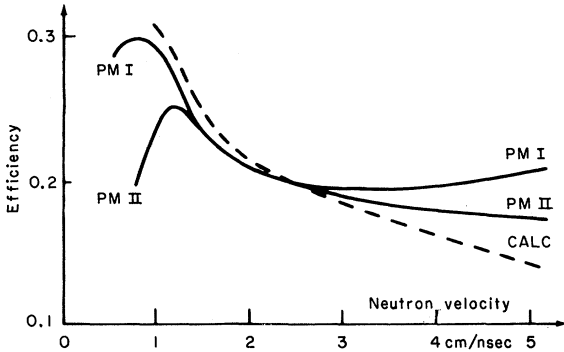


FIG. 4. The "corrected" neutron detection efficiency at 0° to the fragment direction. The dashed curve is the calculated efficiency.

the statistics were very poor (uncommon values of the mass ratio and the total kinetic energy of the two fragments). In these cases, the experimental data could not be corrected for dispersion, and hence the use of an efficiency function based on uncorrected ^{252}Cf data was called for.

We show in Fig. 4 the "corrected" efficiency functions $\epsilon(0^\circ, v)$ for both photomultipliers. The electronic threshold of photomultiplier II was set at higher value than that of photomultiplier I, as it was located in a region of a higher γ background. As a result, the efficiency of II was reduced for low-energy neutrons. In Fig. 4 we also show the calculated efficiency as a function of neutron velocity. The calculation was based on the assumption of a single scattering of the neutron in the scintillator, and no scattering of the neutrons by any other object. The differences between the calculated and the two experimental curves are discussed in Appendix C.

E. Prefission and Postfission Neutrons

We are able to determine the number and velocity distribution of the prefission and postfission neutrons on the basis of the experimentally determined angular and velocity distributions of the neutrons. We assume that the neutrons are either emitted from a stationary (except for the small recoil momentum), excited nucleus in the lab frame or from the fully accelerated fragments. We define the former neutrons as prefission neutrons and the latter as postfission neutrons. (Thus the "scission neutrons,"^{8,16} are included in the prefission neutrons, and we neglect the possibility that neutrons are evaporated from the fragments before those have acquired their final kinetic energy. This is discussed in greater detail in Sec. V.) We further assume that the prefission neutrons are emitted isotropically in the c.m. system of the

fragments. The first assumption is equivalent to the requirement that the prefission neutrons are emitted isotropically in the detector plane i.e., in the plane perpendicular to the beam direction. We do not restrict ourselves in any way with respect to the reaction mechanism prior to fission, or the angular momentum imparted to the target nucleus by the bombarding particle. Furthermore we make no assumptions with respect to the shape of the neutron energy spectrum, except that experimentally we were restricted to the neutron energy range (in the lab system) of 0.5–9.0 MeV.

The neutron spectrum at any angle is composed of three components: (1) prefission neutrons, (2) postfission neutrons from fragment 1, and (3) postfission neutrons from fragment 2. We define the following quantities: θ is the angle with respect to *fragment 1*, and $N(\theta)$ is the neutron spectrum at the angle θ in the lab system. Experimentally the spectrum is given by a column of numbers which denote the number of neutrons at discrete velocity values. We further define:

- (a) $N_i(\text{c.m.})$ is the neutron spectrum in the c.m. of fragment i .
- (b) $N_{b.f.}$ is the prefission neutron spectrum.
- (c) $T(\theta, \text{c.m.}, i)$ is the operator which transforms the neutron spectrum at the lab angle θ to the c.m. of fragment i . The transformation acts differently on each velocity component of $N(\theta)$.
- (d) $T(\text{c.m.}, \theta, i)$ is the operator which transforms the (isotropic) neutron spectrum in the c.m. system of fragment i to the lab angle θ .

The calculation consists of two iterations which yield upper and lower limits of the number of postfission neutrons. The starting points for the two iterations are two extreme assumptions:

- (1) All the neutrons emitted in the fragment direction are postfission neutrons (*upper* limit for postfission neutrons).
- (2) All the neutrons emitted perpendicular to the fragment direction are prefission neutrons (*lower* limit for postfission neutrons).

First Assumption

(Upper Limit for Postfission Neutrons)

We start with the assumption that all neutrons emitted in the direction of fragment 1 ($\theta = 0^\circ$) were emitted from fragment 1; likewise for fragment 2. We obtain for the spectra in the c.m. systems of the two fragments:

$$D^{(0)} N_1(\text{c.m.}) = T(0, \text{c.m.}, 1) N(0), \quad (5a)$$

$$D^{(0)} N_2(\text{c.m.}) = T(180, \text{c.m.}, 2) N(180). \quad (5b)$$

In order to obtain the true c.m. spectra, we must

subtract from Eq. (5a) the contributions of the prefission neutrons and the neutrons emitted from fragment 2 in the direction fragment 1. Similarly, for Eq. (5b).

We calculate the spectrum expected at 90° from the neutrons emitted from fragments 1 and 2 (Eqs. 5a and 5b):

$$N'(90) = T(\text{c.m.}, 90, 1) D^{(0)} N_1(\text{c.m.}) \\ + T(\text{c.m.}, 90, 2) D^{(0)} N_2(\text{c.m.}). \quad (6)$$

The measured spectrum at 90° , $N(90)$, is composed of the prefission neutron spectrum $N(\text{b.f.})$ and the postfission contribution $N'(90)$. Hence

$$N(\text{b.f.}) = N(90) - N'(90). \quad (7)$$

We assumed that $N_{\text{b.f.}}$ is isotropic in the detector plane. Hence the first correction term to Eqs. (5) is given by the contribution of prefission neutrons:

$$D^{(1)} N_1(\text{c.m.}) = -T(0, \text{c.m.}, 1) N_{\text{b.f.}}, \quad (8a)$$

$$D^{(1)} N_2(\text{c.m.}) = -T(180, \text{c.m.}, 2) N_{\text{b.f.}}. \quad (8b)$$

The second correction term (due to neutrons emitted by one fragment in the direction of the other one) is given by

$$D^{(2)} N_1(\text{c.m.}) = -T(0, \text{c.m.}, 1) T(\text{c.m.}, 0, 2) \\ \times [D^{(0)} N_2(\text{c.m.}) + D^{(1)} N_2(\text{c.m.})], \quad (9a)$$

$$D^{(2)} N_2(\text{c.m.}) = -T(180, \text{c.m.}, 2) T(\text{c.m.}, 180, 1) \\ \times [D^{(0)} N_1(\text{c.m.}) + D^{(1)} N_1(\text{c.m.})]. \quad (9b)$$

Thus we obtain at the end of the first iteration a new expression for the postfission spectra:

$$N_f(\text{c.m.}) = D^{(0)} N_f(\text{c.m.}) + D^{(1)} N_f(\text{c.m.}) \\ + D^{(2)} N_f(\text{c.m.}). \quad (10)$$

Equation (10) serves as the starting point for the next iteration. It is still an upper limit for the postfission neutrons. It is, however, lower than our first upper limit, namely, Eqs. (5). Each additional iteration will further reduce this upper limit.

Second Assumption

(Lower Limit for Postfission Neutrons)

We start with the assumption that all neutrons

emitted at 90° to the fission fragments are prefission neutrons (as defined above). In order to obtain the postfission spectrum, we subtract the 90° spectrum from the spectra at 0 and 180° and transform the results to the c.m. system of the two fragments:

$$D^{(0)} N_1(\text{c.m.}) = T(0, \text{c.m.}, 1) [N(0) - N(90)], \quad (11a)$$

$$D^{(0)} N_2(\text{c.m.}) = T(180, \text{c.m.}, 2) [N(180) - N(90)]. \quad (11b)$$

The rest of the procedure is identical with that of Assumption I except that Eqs. (11) are substituted for Eqs. (5). The result will be a lower limit for the postfission spectrum, since we started with the assumption that the spectrum at 90° is due to prefission neutrons only. The details of the calculation are discussed in Appendix D.

In this fashion we obtain upper and lower limits for the postfission spectrum. The difference between the two limits could in principle be reduced to any given limit. In practice, it is meaningless to try to narrow the difference below the size of the statistical and systematic errors. In our experiment these limits were reached after one iteration.

The above procedure determines the number and energy spectrum of the postfission neutrons. It also determines the energy spectrum of the prefission neutrons in the detector plane (i.e., perpendicular to the beam of direction). In order to obtain the total number of prefission neutrons (excluding the neutrons emitted during the fast intranuclear cascade), we make the additional assumption that the prefission neutrons are emitted isotropically in the lab system.

The justification for this assumption is further discussed in Sec. V.

F. Calculation

We have seen that the evaluation of the number and the energy spectrum of the postfission neutrons involves transformations of the lab neutron spectra at 0, 90° , and 180° to the c.m. system of the fragments. These transformations require the knowledge of the fission fragment velocity and the neutron velocity for each event. For this purpose we sorted all events into a three-dimensional matrix of "bins." The three dimensions were: (1) the mass of the fission fragment A_f , (2) the total kinetic energy of the two fragments E_K , and (3) the neutron flight time t . (Since we assume a fissioning nucleus of a given mass value, the fragment

velocity is determined by the total energy E_K and the fragment mass.) The "mass-energy plane" was divided into 280 mass-energy bins (this number was determined by the size of the computer memory and the actual number of intervals in the mass, and the energy dimensions were chosen to be optimum for the particular calculation at hand). For each bin in the mass-energy plane there was a "complementary" bin with the same value of E_K and complementary mass value (see Fig. 5). The 0° spectrum corresponded to the 180° spectrum in the complementary bin, and the 90° spectra were the same for the two bins. The "size" of the bins was increased towards the edges of the distributions because of the low number of events in these bins. The finite extent of the mass-energy bins introduced a dispersion in the fragment velocity associated with the bin. However, this dispersion had in most cases a standard deviation of less than 1% of the fragment velocity. For each "bin" we recorded the fragment velocity value and its standard deviation, the relative fission yield, and 48 intervals of the neutron time-of-flight spectrum at 0 and 90° to the fragment. Only "zero time" corrections were performed on the time-of-flight data in each mass-energy bin, since the total number of counts in each bin was low. We used therefore the "uncorrected" effective efficiency curve for these data. The subtraction of the random events was performed by subtracting from each time-of-flight spectrum in a given mass-energy bin the total random spectrum multiplied by the relative fission yield of that bin. In this fashion the number of postfission neutrons $\nu(A_f, E_K)$ associated with each bin was obtained. $\nu(A_f)$ and $\nu(E_K)$ were obtained by summing over columns and rows, respectively, the values of $\nu(A_f, E_K)$ weighted by the relative fission yield of each bin. Finally, the total number of postfission neutrons was obtained

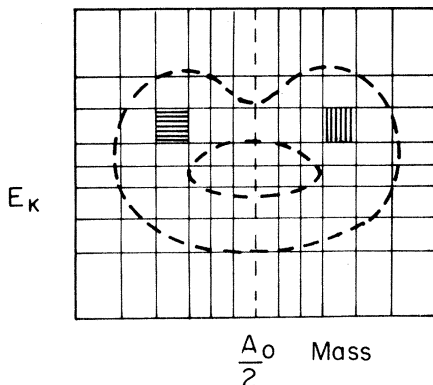


FIG. 5. Schematic drawing of the mass-energy matrix. The dotted lines indicate mass-energy contours of equal yields.

by summing in this manner over all rows and columns.

The total number of postfission neutrons was also calculated from the total time-of-flight spectrum, without division into mass-energy bins. In this case, all the corrections which were discussed in (C) above were applied to the data in addition to random subtraction and zero-time correction. The average fragment velocity was used for the transformation to the c.m. system of the fragments. The results for the total number of prefission and postfission neutrons obtained by this method agree within the statistical error with the results based on mass-energy bins.

We also checked the consistency of our results by transforming the calculated postfission spectrum for U to 30 and 60° lab angle and adding the prefission spectrum. The results were compared with the experimental spectra measured at these angles. Good agreement was obtained.

IV. EXPERIMENTAL RESULTS

A. Neutron Spectrum in the Lab System

The lab neutron spectrum at 0 , 30 , 60 , and 90° with respect to the fragment direction for the ^{238}U target, and the lab neutron spectrum at 0 and 90° for the ^{209}Bi target are shown in Fig. 6. The statistical corrections to the time-of-flight data which were discussed in the previous section have been applied to the spectra shown in this figure. The

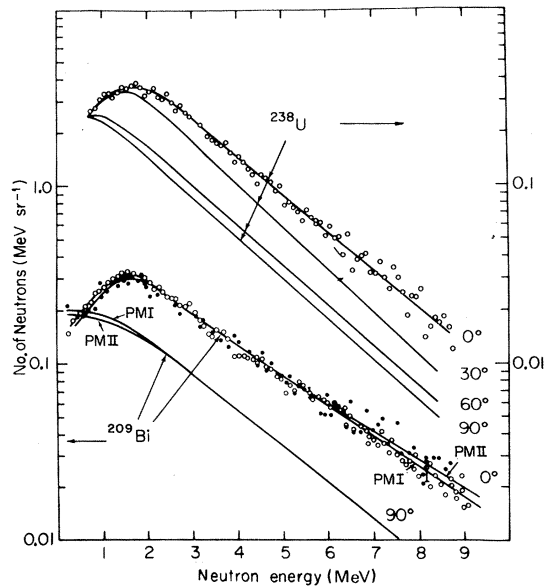


FIG. 6. The lab neutron spectra at 0 , 30 , 60 , and 90° with respect to the fission fragment direction for U and at 0 and 90° for Bi.

TABLE I. The number of neutrons/sr per fission event at various angles with respect to the fission fragment direction for $^{209}\text{Bi} + 155\text{-MeV } p$, $^{238}\text{U} + 155\text{-MeV } p$ (this experiment), $^{235}\text{U} + n_{\text{th}}$ (see Ref. 16), and spontaneous fission of ^{252}Cf (see Ref. 8).

Neutrons/sr	$^{209}\text{Bi} + 155\text{-MeV } p$	$^{238}\text{U} + 155\text{-MeV } p$	$^{235}\text{U} + n_{\text{th}}$	^{252}Cf (S.F.)
$N(0^\circ)$	1.11 ± 0.03	1.22 ± 0.03	0.399 ± 0.002	0.8
$N(30^\circ)$		1.06 ± 0.03	0.259 ± 0.002	0.40 ± 0.01
$N(60^\circ)$		0.70 ± 0.03	0.101 ± 0.001	0.205 ± 0.005
$N(90^\circ)$	0.63 ± 0.03	0.59 ± 0.03	0.064 ± 0.001	0.120 ± 0.002
$N(0^\circ)/N(90^\circ)$	1.77	2.05	6.1	6.6

spectra were obtained on the basis of the corrected effective efficiency derived from the measurement of the neutron spectrum of ^{252}Cf at 0° with respect to the fragment. It is shown in Appendix C that the use of the 0° effective efficiency for the U and Bi neutron spectra at all angles results in an overestimate of the non- 0° spectra. The largest overestimate is that of the 90° data. The total number of neutrons per fission and per sr at the various angles with respect to the fragment direction and the ratio of the number of neutrons at 0° to that at 90° are given in Table I. The number of neutrons in this table pertain to neutrons in the energy range 0.5–9.0 MeV, i.e., the energy range detected in our experiment. For comparison we also show the numbers for thermal-neutron fission of ^{235}U , obtained by Skarsvåg and Bergheim,¹⁷ and those of the spontaneous fission of ^{252}Cf of Bowman *et al.*⁸ Since the 0° efficiency curve was used for all angles, the non- 0° neutron numbers for ^{238}U and ^{209}Bi are overestimates, whereas the $0^\circ/90^\circ$ values are underestimates of the true values. If the 90° data are analyzed on the basis of the 90° efficiency curve one obtains values for the $0^\circ/90^\circ$ ratio which are larger by 20% than those given in Table I. On this basis we estimate the actual error to be less than 10% for the 90° and $0^\circ/90^\circ$ data, and smaller for the other angles. (See also Appendix C.)

In Table II we present the average neutron energies for neutrons in the energy range 0.5–9.0 MeV. The angles and targets are the same as in Table I. The 0° efficiency curve was used to obtain the average energies.

TABLE II. The average kinetic energy of the neutrons at various angles with respect to the fission fragment direction for $^{209}\text{Bi} + 155\text{-MeV } p$, $^{238}\text{U} + 155\text{-MeV } p$ (this experiment), $^{235}\text{U} + n_{\text{th}}$ (see Ref. 16), and spontaneous fission of ^{252}Cf (see Ref. 8).

Neutron energy (MeV)	$^{209}\text{Bi} + 155\text{-MeV } p$	$^{238}\text{U} + 155\text{-MeV } p$	$^{235}\text{U} + n_{\text{th}}$	^{252}Cf (S. F.)
$\bar{\epsilon}(0^\circ)$	3.02	3.10	2.61	3.00
$\bar{\epsilon}(30^\circ)$		2.60	2.30	2.65
$\bar{\epsilon}(60^\circ)$		2.45	1.86	2.36
$\bar{\epsilon}(90^\circ)$	2.45	2.42	1.65	2.10

B. Number of Prefission and Postfission Neutrons

The number of postfission neutrons was calculated by the iterative procedure which was described in the previous section. The number of prefission neutrons was calculated with the additional assumption that these neutrons are emitted isotropically in the lab system. The results are presented in Table III. The numbers of prefission and postfission neutrons were calculated using both the 0° and the 90° efficiency curves for the 90° data, and the numbers shown in Table III are the averages of the results obtained on the basis of these two procedures. The difference between the two results is about 10% for the postfission neutrons, and it constitutes the maximum systematic error in the postfission neutron numbers of Table III due to the uncertainties of the neutron detection efficiency. The maximum systematic error for the prefission neutrons is $\pm 20\%$. This difference in the systematic error is due to the smaller weight of the 90° data in the calculation of the postfission neutrons.

Table III shows the results for the two initial assumptions (I. All 0° neutrons are postfission neutrons, and II. 90° neutrons are prefission neutrons) and the results after one iteration for each of the two assumptions. The results based on the two initial assumptions are given only for comparison. (They do not constitute a valid first approximation since the values obtained for the prefission and postfission neutrons for each assumption are not consistent with each other. Thus the number of

TABLE III. The average number of prefission and postfission neutrons for Bi and U under assumption No. 1 (upper limit of postfission neutrons) and assumption No. 2 (lower limit of postfission neutrons). The results before and after the first iteration are shown. The estimated uncertainties are ± 1.0 neutron for prefission and ± 0.5 neutron for postfission neutrons (both Bi and U).

Assumption and iteration	$^{209}\text{Bi} + 155\text{-MeV } p$		$^{238}\text{U} + 155\text{-MeV } p$	
	prefission	postfission	prefission	postfission
No. 1, no iter.	4.90	6.02	4.05	6.64
No. 1, one iter.	6.01	4.06	5.12	4.82
No. 2, one iter.	6.13	3.67	5.44	4.56
No. 2, no iter.	7.75	3.20	7.45	4.08

prefission neutrons obtained with assumption I is not zero, but the number of postfission neutrons was not corrected accordingly). The estimated uncertainty in the values of Table III are ± 0.5 neutrons for the postfission neutrons and ± 1.0 neutrons for the prefission neutrons. These uncertainties are due to statistical errors, and the estimates of the systematic errors and errors due to the scattering effects (see Appendix C). The difference between the results of the upper- and lower-limit assumptions after one iteration is smaller than the estimated error in the results. Therefore no additional iteration was performed. The mean of the upper- and lower-limit results after one iteration constitutes the "best" result.

Another correction which must be considered is the effect of the neutrons outside our limits of detection, i.e., neutrons of energy below 0.5 MeV and above 9.0 MeV. This effect is estimated in Appendix E. By assuming a rectangular distribution of the initial excitation energy of the fragments and a level-density parameter which reproduces the neutron spectrum and the average number of neutrons, we arrive at the estimate that 8% of the postfission neutrons in both the ^{238}U and ^{209}Bi experiments have a lab energy above 9.0 MeV, and were therefore not detected in our experiment. Similarly 7% of the prefission neutrons had an energy below 0.5 MeV and therefore were not counted by our system. The effect of the lower detection limit on the postfission neutrons and of the upper limit on the prefission neutrons is negligible.

The final "best" results are the following: U, 4.7 ± 0.5 postfission neutrons within the experimental detection range, and altogether 5.1 ± 0.5 postfission neutrons; Bi, 3.8 ± 0.5 postfission neutrons within the experimental detection range, and altogether 4.2 ± 0.5 postfission neutrons.

The best values for prefission neutrons, including corrections for neutrons outside the experimental detection limits, are 5.8 ± 1.0 for U and 6.9 ± 1.0 for Bi. We reiterate that the prefission neutrons numbers were obtained by assuming an isotropic spectrum in the lab system for these neutrons.

The total number of prefission and postfission neutrons is 11.1 ± 1.0 for Bi and 10.9 ± 1.0 for U. These numbers are in good agreement with the results obtained by integrating the laboratory angular distributions (10.9 ± 1.0 for Bi and 11.4 ± 1.0 for U). Our results for the total number of neutrons are in reasonable agreement with the results of Harding,² who obtained 13.1 ± 1.8 neutrons for U and 10.0 ± 2.7 neutrons for Bi at a bombarding energy of 147 MeV.

It should be stressed that our results for the number of prefission and postfission neutrons were obtained without reference to any model of fission-spallation competition or of neutron evaporation (e.g., the statistical model). The neutron spectra were not fitted to any theoretical spectrum except for the evaluation of the effect of the upper limit of detection. Since this effect amounts to less than 10% of the number of postfission neutrons, other assumptions with respect to the neutron spectrum would result in a difference smaller than our stated errors.

C. Energy Spectra of the Prefission and Postfission Neutrons

The energy spectra of the prefission and postfission neutrons from U and Bi, as obtained from the iteration procedure, are shown in Fig. 7. The prefission spectra refer to the lab system, whereas postfission spectra refer to the c.m. system of the fragments. The curves show the spectra obtained after the first iteration and using the 0° efficiency curve for the lab spectra at both 0 and 90° . The first-order correction (difference between zero-order and first-order iteration) for the lower-limit assumption (Assumption II) is also shown in Fig. 7. The experimental upper limit of 9.0 MeV in the lab neutron energy results in a 5.2-MeV upper limit for the postfission neutron. This artificial cutoff also affects the first-order correction to the prefission spectra, and is the reason for the discontinuities in these spectra around 5.2 MeV. It is seen that the prefission neutrons have higher average energies than the postfission neutrons, in

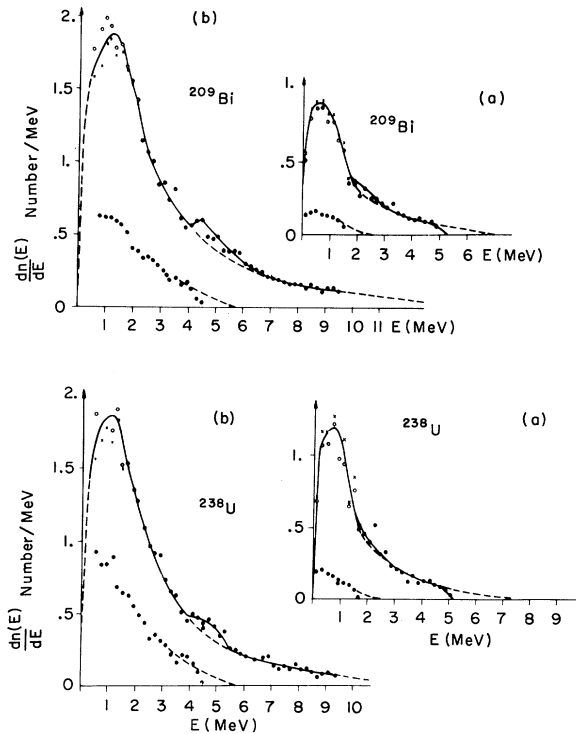


FIG. 7. The prefission and postfission neutron spectra for Bi and U: (a) Postfission neutron spectra; (b) prefission neutron spectra. Hollow circles refer to results of upper-limit assumption after first iteration, crosses to results of lower-limit assumption after one iteration. Solid circles are for mean values between upper- and lower-limit assumptions after first iteration. The data in the lower left side of each graph show the magnitude of the first-order correction to the lower-limit assumption (difference between zero- and first-order iteration).

qualitative agreement with the notion that the prefission neutrons are emitted at higher excitation energies (higher nuclear temperatures) than the postfission neutrons.

D. Dependence of the Number of Prefission and Postfission Neutrons on the Fragment Mass

The average number of prefission and postfission neutrons as a function of the mass division was obtained by summing over all kinetic-energy rows in the mass-energy matrix and adding complementary mass values. The results for the total number of neutrons, the prefission neutrons and postfission neutrons, as a function of the mass division are shown in Fig. 8. The total number of neutrons seems to be independent of the mass ratio for Bi and seems to drop slightly with increasing mass ratio for U. The number of prefission neutrons decreases with increasing mass ratio for both Bi and U, whereas the number of postfission neutrons

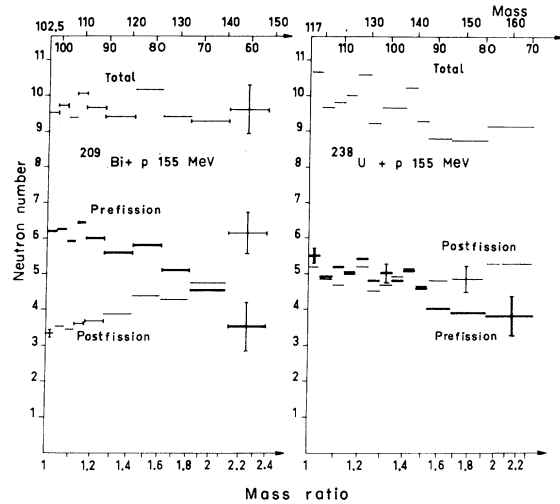


FIG. 8. The number of prefission and postfission neutrons and the total number of neutrons as a function of mass division.

increases with the mass ratio for Bi and is roughly independent of the mass ratio for U. The results for Bi seem to indicate that the larger mass ratios are associated with fission at higher excitation energy (earlier in the neutron-evaporation cascade), i.e., the width of the mass distribution increases with increasing excitation energy at the moment of fission. The situation is more complicated for U because of the effect of low-energy fission.

The average number of postfission neutrons as a function of the fragment mass is shown in Fig. 9. In this figure we show the result obtained by the zero-order upper limit (max) and the zero-order lower limit (min). The results after one iteration for both the upper- and lower-limit assumptions are shown by the pair of dashed lines close to each other and between the "min" and "max" lines. The average between the "first-iteration" lines corrected for the missing part of the spectra is shown by the solid lines, which represent the best estimate of the final result. The statistical error (based only on counting statistics) and the mass distribution (dotted line) are also shown. The curves of Fig. 9 were calculated by using the 0° effective efficiency curve for all angles. The use of the 90° efficiency curve for the 90° data results in a slight upward shift of the curves, but does not alter their shapes or their typical dependence on the fragment mass.

The basic feature of Fig. 9 is the rapid increase in the number of neutrons with mass number. The fast rise of $\bar{\nu}(A_f)$ seems to indicate that the average nuclear temperature increases with the mass number. Support for this conclusion is shown in Fig. 10, where we show the average kinetic energy of

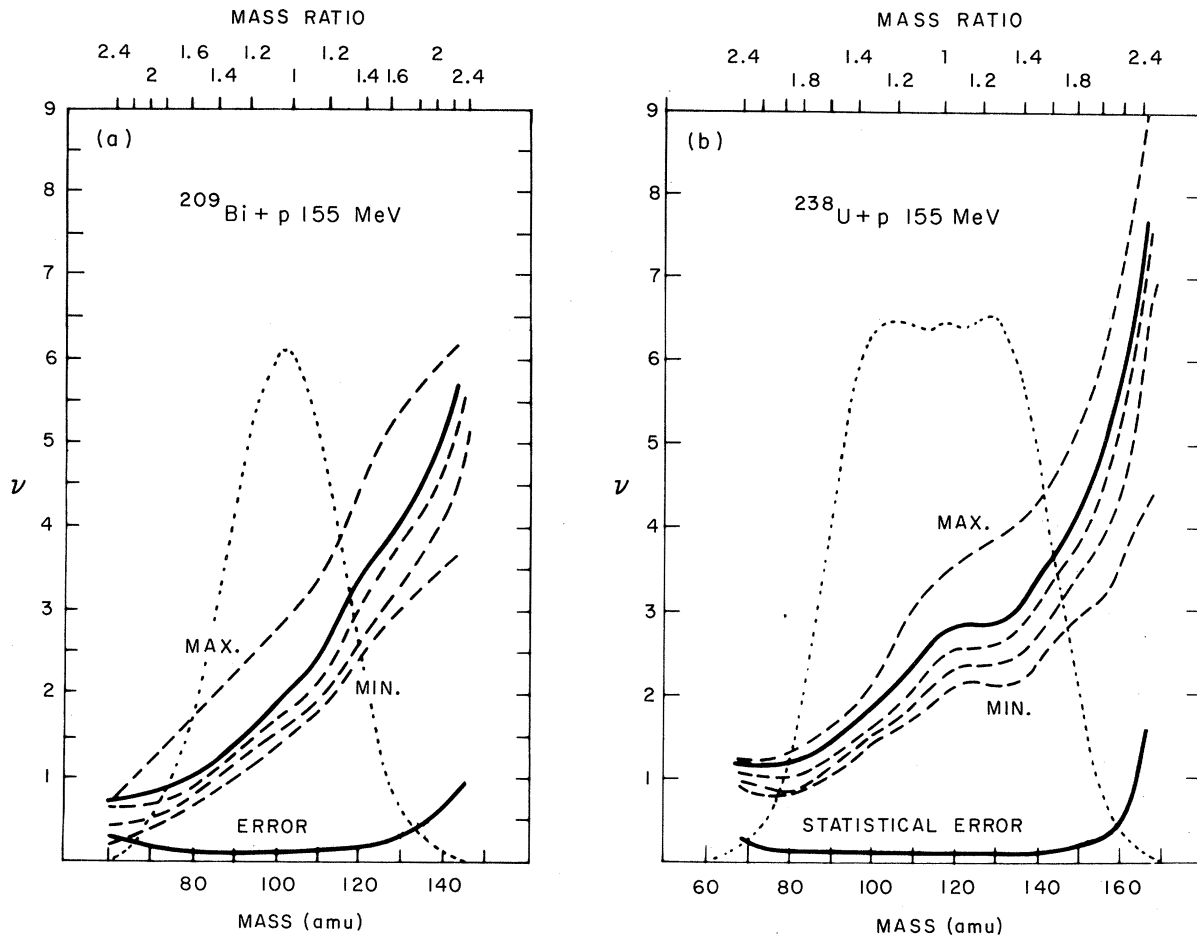


FIG. 9. (a), (b) The average number of postfission neutrons $\bar{\nu}(A)$ as a function of fragment mass. Max, result for zero-order upper-limit assumption. Min, result for zero-order lower-limit assumption. The two dashed lines between the Max and Min lines are the results of the first iteration of the upper-limit and lower-limit assumptions. The solid lines are the mean of the two latter lines corrected for neutrons outside the experimentally measured velocity limits. They constitute the final results of the experiments.

the postfission neutrons in the c.m. system of the fragment as a function of fragment mass. We see that the average c.m. kinetic energy of neutrons increases with the fragment mass number. Since for an evaporation spectrum the average energy is proportional to the nuclear temperature T , Fig. 10 seems to indicate an increase in T with fragment mass.

Comparing the $\bar{\nu}(A_f)$ curves for U and Bi (Fig. 9) one sees a flattening of the $\bar{\nu}(A_f)$ curve around mass $A_f=130$ in U, whereas no such flattening is seen in Bi. The flattening in U appears at a mass region where the dip occurs in the well-known saw-tooth curve of $\bar{\nu}(A_f)$ for thermal-neutron fission. Such a dip is also seen in fission of ^{238}U bombarded with 12-MeV protons.¹⁸ It is therefore possible that the flattening in the ^{238}U curve of Fig. 9 results from

low-energy fission events. Thus the total mass distribution for ^{238}U bombarded by 155-MeV protons is symmetric, however the mass distribution for events of high total kinetic energy of the two fragments is slightly asymmetric.¹⁹ The average number of postfission neutrons as a function of fragment mass for events of high total kinetic energy ($E_K > 171$ MeV for U and $E_K > 156$ MeV for Bi), and for low total kinetic energy ($E_K < 154.5$ MeV for U and $E_K < 135.5$ MeV for Bi) are shown in Fig. 11. The high- E_K data for U show distinct flattening at mass $A_f=130$, whereas the low- E_K data for U and both the high- and low- E_K data for Bi do not show this flattening. Both the absolute number as well as the rate of increase of the number of neutrons with mass is higher for low- E_K events than for high- E_K events.

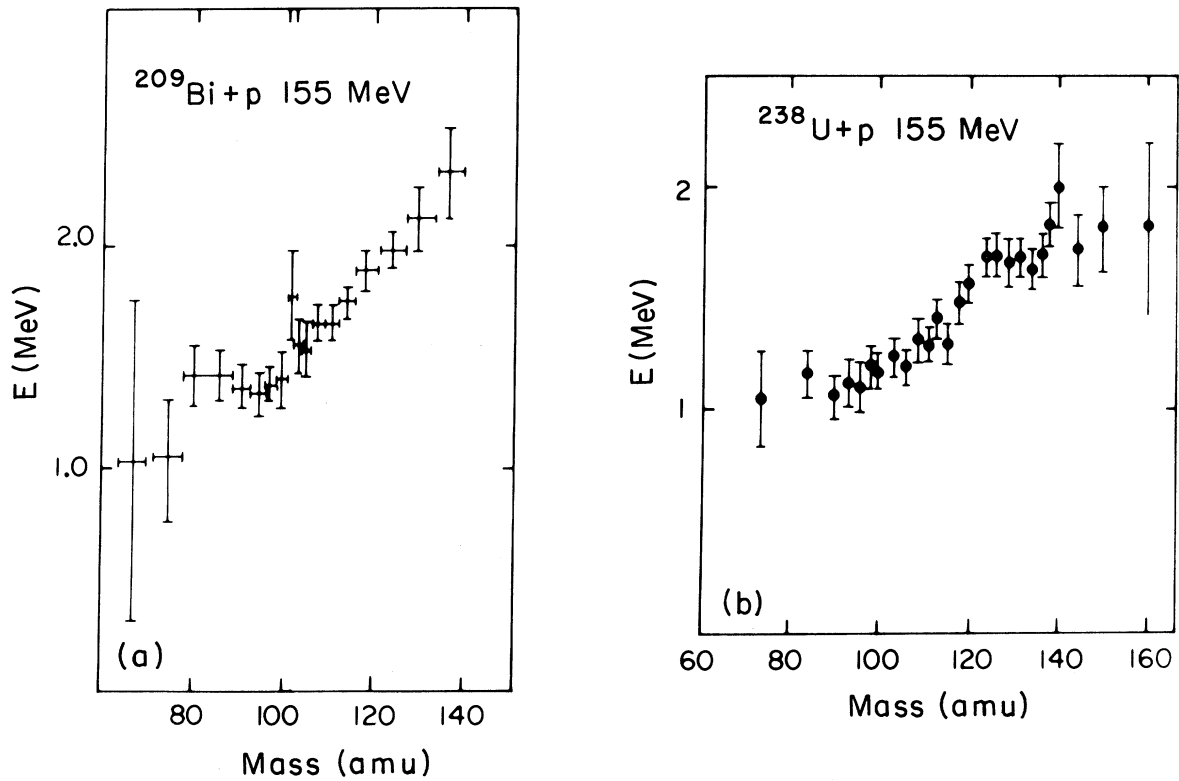


FIG. 10. (a), (b) The average kinetic energy of the postfission neutrons in the c.m. system of the fragment as a function of the fragment mass.

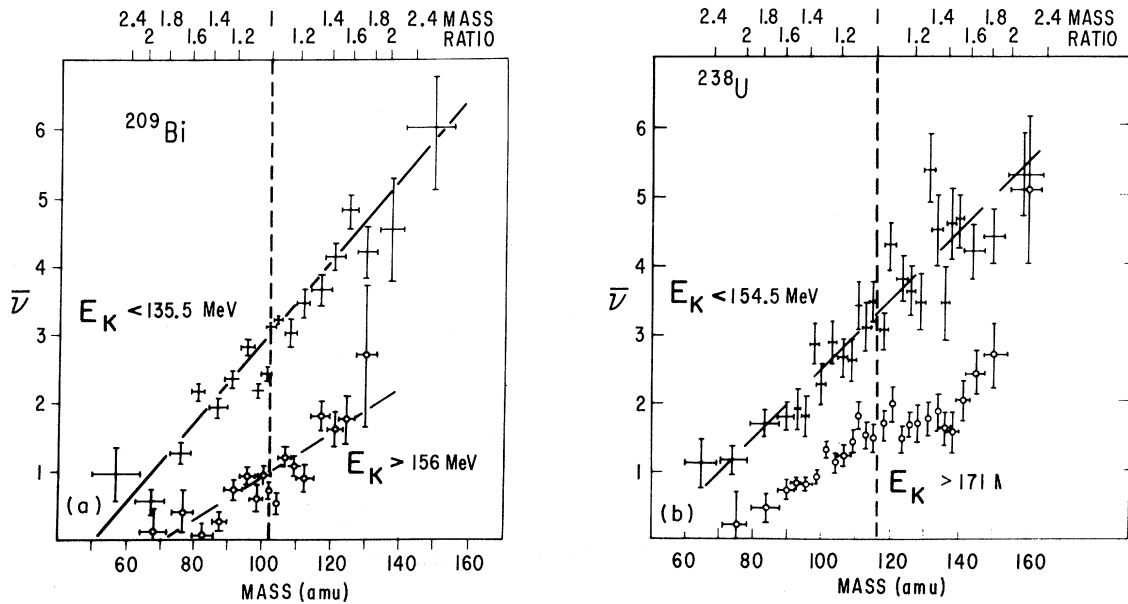


FIG. 11. (a), (b) The average number of postfission neutrons as a function of the fragment mass for events of high total kinetic energy E_K of the two fission fragments and for events with low E_K .

E. Dependence of the Number of Postfission Neutrons on the Kinetic Energy of the Fragments

The average number of postfission neutrons as a function of the total kinetic energy of the fragments $\bar{\nu}(E_K)$ was obtained by summing the mass-energy matrix $\bar{\nu}(A_f, E_K)$ over the mass columns with the weights of the fission yield. $\bar{\nu}(E_K)$ is of interest since it represents the correlation between the deformation energy of the nucleus and the total kinetic energy of the fragments. This statement is correct only when $\bar{\nu}(E_K)$ is measured for a given mass division, since \bar{E}_K is also a function of the mass division. We have attempted to eliminate this effect to a large extent by calculating $\bar{\nu}(E_K)$ for the mass regions for which \bar{E}_K is approximately constant, i.e., $95 < A_f < 140$ for U and $85 < A_f < 120$ for Bi.¹⁹ The results are shown in Fig. 12. The

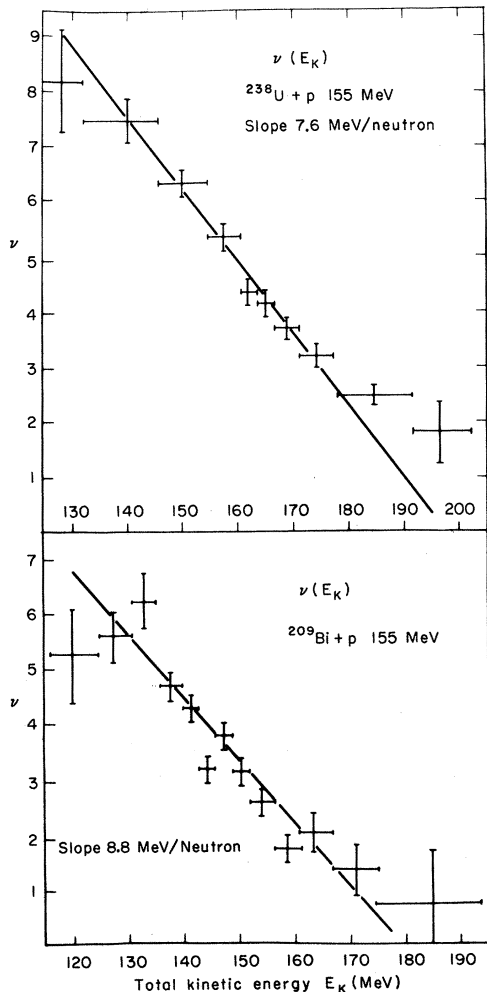


FIG. 12. The average number of postfission neutrons as a function of the total kinetic energy of the two fission fragments.

average slope $\bar{\nu}(E_K)$ is 7.6 MeV/neutron for U and 8.8 MeV/neutron for Bi. Assuming this slope to represent the average energy taken away by each postfission neutron we see that the average total excitation energy of the fission fragments required for neutron emission is 39 MeV for U and 37 MeV for Bi. In order to obtain an estimate to the average excitation energy of the fissioning nucleus, we must subtract from these numbers the deformation energy of the fission fragments.

An estimate of the average excitation energy E_0^* of the fissioning nucleus may be obtained from the relation

$$\bar{E}_0^* = \bar{\nu}\bar{E}_n^* + \bar{E}_\gamma + \bar{E}_K + \bar{\Delta M},$$

where \bar{E}_n is the average energy spent on the emission of one postfission neutron, \bar{E}_γ is the total energy spent on emission of γ rays, and $\bar{\Delta M}$ is the average mass difference between the (ground-state) fissioning nucleus and the (ground-state) fission fragments prior to neutron emission. For symmetric fission of ^{234}U and ^{205}Po , we assume $\bar{\Delta M} = 191.8$ MeV and 149.8 MeV, respectively.²⁰ The total kinetic energy of the fission fragments is $\bar{E}_K = 166$ MeV and 149 MeV, respectively, for U and Bi.¹⁹ We assume $\bar{E}_\gamma = 9$ MeV in both cases. These values yield for the average excitation energy prior to fission $\bar{E}_0^* = 21$ MeV for U and 44 MeV for Bi. However, these numbers should not be taken to be more than rough estimates of \bar{E}_0^* , in view of the uncertainty of the values of $\bar{\Delta M}$, E_n , and E_γ .

V. DISCUSSION

A. Evaluation of the Assumptions Concerning Neutron Emission

1. Prefission and Postfission Neutrons: Experimental Definition

The analysis of our experimental results is based on the division of all the neutrons accompanying a fission event into two groups:

(a) *Prefission neutrons*, which are assumed to be emitted from the stationary (except for the recoil momentum) excited nucleus, and which are not correlated with the fragment direction. In order to calculate the total number of prefission neutrons, we make the additional assumption that the prefission neutrons are emitted isotropically from the excited nucleus.

(b) *Postfission neutrons*, which are assumed to be emitted isotropically from the fully accelerated fragments.

Several questions arise with respect to these

assumptions:

(1) How many neutrons are emitted while the fissioning system is at the saddle point (transition point) and in the stage between the saddle and scission points?

(2) How many neutrons are emitted during scission?

(3) How many neutrons are emitted from the moving fragments before they are fully accelerated?

(4) To what extent are our assumptions regarding the isotropy of emission of the prefission neutrons in the detector plane (perpendicular to the beam direction) and the isotropy of emission of the postfission neutrons from the fragments justified?

It is immediately seen that our questions fall into two categories: (a) The first two questions concern the *interpretation* of correctly analyzed experimental results. According to our experimental definition, neutrons which are emitted before or during scission are prefission neutrons whereas, as shall be discussed below, the neutrons referred to in (1) and (2) should probably be regarded as postfission neutrons. (b) The last two questions concern the possibly incorrect *analysis* of our experimental results.

2. Postfission Neutrons Emitted before Full Acceleration of the Fragments

(a) *Neutrons emitted at the saddle point or between saddle and scission points.* The experimental definition of prefission and postfission neutrons as emitted from the stationary excited nucleus and from the fully accelerated fragments, respectively, is not completely compatible with the definition of these neutrons according to the statistical theory of nuclear reactions. According to this theory the relative probability of fission versus neutron emission is given by the number of open channels to fission versus the number of open channels for neutron emission. The number of open channels for fission is taken to be the number of available levels for the excited system above the saddle point. It is therefore implicitly assumed that once the system has reached the saddle point, it will undergo fission. The neutrons which are emitted while the system is in the transition state (i.e., at the saddle point) or beyond that point are therefore to be regarded as postfission neutrons according to the statistical model. The time which the fissioning system spends at the saddle point may be estimated in the following way. For a system of mass m and energy E above the top of a parabolic barrier $V = -\frac{1}{2}Cx^2$, the time t it takes the system to travel from $-x_f$ to x_f (x is the fission direction, with $x=0$ at the top of the barrier) is given by

$$t = 2 \int_0^{x_f} \frac{dx}{[(2/m)(E + \frac{1}{2}Cx^2)]^{1/2}} = \frac{2}{|\omega_f|} \times \ln \left[\left(\frac{\frac{1}{2}Cx_f^2}{E} \right)^{1/2} + \left(1 + \frac{Cx_f^2}{E} \right)^{1/2} \right],$$

where $|\omega_f| = \sqrt{C}/m$ is the absolute value of the (imaginary) frequency of the system in the fission direction. For $E = \frac{1}{2}Cx_f^2$ we obtain $t = 2|\omega_f|^{-1} \ln(1 + \sqrt{2})$. Liquid-drop-model calculations of Nix²¹ yield approximately 2×10^{-21} sec for this number. This time will be shorter for higher excitation energies.

The transition time from the saddle point to the scission point may again be estimated from the liquid-drop-model calculations of Nix²¹ for non-viscous irrotational flow. (For a given path, this type of flow requires the minimum time, since either viscosity or an increase in mass increases the time.) He finds that for systems starting at the saddle point with 1 MeV of kinetic energy in the fission mode, this transition time is approximately 2×10^{-21} sec for Bi and 3×10^{-21} sec for U. This time interval will again be shorter for more highly excited nuclei. The total time that the system spends at the saddle point and from saddle point to scission point is therefore less than 10^{-20} sec.

The neutron emission width is given according to evaporation theory²²

$$\Gamma_n = \frac{A^{2/3}(E^* - B_n)}{a_n \pi K_0} \exp [2a_n^{1/2}(E^* - B_n)^{1/2} - 2(a_c E^*)^{1/2}]. \quad (12)$$

Here A is the mass of the excited nucleus; E^* - the excitation energy; B_n - the neutron binding energy; a_c and a_n - level-density parameters of the compound nucleus and the residual nucleus, respectively, and K_0 a constant ($K_0 \approx 10$ MeV). Assuming $a_n = a_c = A/10$ MeV⁻¹, $A = 240$, and $B_n = 6$ MeV, we obtain for the neutron lifetime $\tau_n = \hbar/\Gamma_n$ in the case of $E^* = 50$ MeV a value of $\tau_n = 2 \times 10^{-20}$ sec, whereas for $E^* = 25$ MeV we obtain $\tau_n = 4 \times 10^{-19}$ sec. Assuming $a_n = a_c = A/20$ MeV⁻¹, we obtain $\tau_n = 3 \times 10^{-21}$ sec and 3×10^{-20} sec for $E^* = 50$ and 25 MeV, respectively. Using a rather different model²³ to calculate the neutron emission times, J. M. Miller²⁴ obtains values comparable to the evaporation model results with $a_n = a_c = A/10^{-1}$. It should be remembered that in our case E^* is the excitation energy *above the fission barrier*, and the above values of E^* correspond to a total excitation energy of ~ 55 and ~ 30 MeV, respectively, in the case of U and considerably higher values in the case of Bi. In

the preceding section we estimated that the average total excitation energy of the excited nucleus at the moment of fission is approximately 21 MeV for U and approximately 44 MeV for Bi. We may therefore conclude that if this estimate is correct, the probability of neutron emission between the time the system reaches the saddle point to the moment of scission is quite small. If, on the other hand the average excitation energy is much higher, this probability is no longer negligible.

(b) *Scission neutrons.* The existence of scission neutrons was suggested by Bowman *et al.*,⁸ in order to explain their experimental results. They suggested that the scission neutrons are emitted isotropically from the fissioning nucleus at the moment of scission. Moreover, various charged particles are known to be emitted in fission, and their angular distribution indicates that they are emitted from the neck region between the two fragments at the moment of scission.²⁵ It would therefore be surprising if neutrons were not emitted at scission. Bowman *et al.* estimated the number of scission neutrons in the spontaneous fission of ²⁵²Cf to be approximately 0.4 neutrons/fission. Milton and Fraser²⁶ estimated that as many as 30% of all the neutrons emitted in the thermal-neutron fission of ²³³U and ²³⁵U might be scission neutrons. The results of Loveland, Fairhall, and Halpern²⁷ show that the number of α particles emitted in fission is roughly independent of the excitation energy of the fissioning nucleus up to $E_0^* = 35$ MeV (the highest energy which they measured). Assuming the same to be true for the scission neutrons, we estimate that 0.4–1.0 scission neutrons/fission were emitted in our experiment. They are classified as pre-fission neutrons in our analysis.

(c) *Neutrons emitted during the acceleration of fragments.* Postfission neutrons may be emitted from the fragments before these are fully accelerated. In this case, fewer neutrons are detected in the direction of the fission fragments than in the case where they are emitted from the fully accelerated fragments. If the experimental results are analyzed on the assumption that all postfission neutrons are emitted from the fully accelerated fragment, the analysis will yield a smaller number of postfission neutrons than were actually emitted. We shall try to estimate the error in our experiments due to this fact. In this, we shall follow the approach of Eismont.²⁸

Let the neutron spectrum in the c.m. system of the moving fragment be $N(v_{c,m.}) dv_{c,m.}$, where $v_{c,m.}$ is the neutron velocity in the c.m. system of the fragment. The Jacobian of the transformation to the lab system is $(v_{c,m.} + v_f)^2/v_{c,m.}^2$, where v_f is the fragment velocity at the moment of neutron emission. The Jacobian of the transformation from

the lab system to the system of the fully accelerated fragment of velocity v_∞ is $(v_{c,m.} + v_f - v_\infty)^2/(v_{c,m.} + v_f)^2$. The calculated spectrum is therefore

$$N(v')dv' = N(v_{c,m.}) [(v_{c,m.} + v_f - v_\infty)^2/v_{c,m.}^2] dv_{c,m.}, \quad (13)$$

where v' is the neutron velocity in the c.m. system of the fully accelerated fragment. We assume the neutron spectrum to have a Maxwellian form

$$N(v_{c,m.}) dv_{c,m.} = \frac{2v_{c,m.}^3}{v_0^4} \exp[-V_{c,m.}^2/V_0^2] dv_{c,m.}. \quad (14)$$

v_0 is a constant which depends on the nuclear temperature (excitation energy). The time distribution of neutron emission from the excited fragment is

$$P(t) = (1/\tau_n) e^{-t/\tau_n}, \quad (15)$$

where $\tau_n = t/\Gamma_n$, and the neutron emission width Γ_n is given by Eq. (12).

The calculated number of neutrons emitted from a fragment for the first neutron actually emitted from this fragment is given by

$$\begin{aligned} \epsilon(E^*) = & \int_0^{v_\infty} \int_{v-v_f}^{\infty} P(t, E^*) \frac{\partial t}{\partial v_f} N(v_{c,m.}, E^*) \\ & \times \frac{(v_{c,m.} + v_f - v_\infty)^2}{v_{c,m.}^2} dv_{c,m.} dv_f \end{aligned} \quad (16)$$

[Both $P(t)$ and $N(v_{c,m.})$ are functions of the excitation energy E^* through their dependence on τ_n and v_0 , respectively]. The integration with respect to $v_{c,m.}$ is carried out to infinity rather than for the maximum possible velocity $[2(E^* - B_n)/m]^{1/2}$. This introduces a negligible error in the calculation. (A similar integral may be written for the second and the following neutrons except that E^* is then the excitation energy of the fragment after the emission of the previous neutrons, and that the lower limit of the integration with respect to v_f is then the fragment velocity at the time of emission of the previous neutron.) We obtain

$$\begin{aligned} \epsilon(E^*) = & \int_0^{v_\infty} P(t, E^*) \frac{\partial t}{\partial v_f} \{e^{-\chi_0^2} (1 + \chi_0^2) \\ & - \pi^{1/2} \chi_0^2 [1 - \text{erf}(\chi_0)]\} dv_f, \end{aligned} \quad (17)$$

where $\chi_0 = (v_{c,m.} - v_f)/v_0$.

To a good approximation the fragment lab velocity v_f is the velocity, as function of time, of point charges which are at rest at the moment of scission and have a total kinetic energy E_K at infinity.

Nix²¹ has shown that the fragments already have an appreciable part of their final velocity at the moment of scission. Hence our calculation starts before the actual moment of scission. (This means that our estimate of the number of neutrons emitted before the fragments start to move [see part 2(b) above] is an overestimate of the true number.)

The relation between the distance r between the fragments and the lab velocity v_f of fragment A_1 is given by

$$r/r_0 = [1 - (v_f^2/v_\infty^2)]^{-1}, \quad (18)$$

where r_0 is the distance between the fragments at rest ("scission distance") and v_∞ is the lab velocity of fragment A_1 at infinity. We have

$$\frac{A_2}{A_0} dr = v_f dt = r_0 \frac{A_2}{A_0} \frac{2(v_f/v_\infty^2)}{[1 - (v_f/v_\infty^2)]^2} dv_f, \quad (19)$$

where A_2 is the mass of the complementary fragment and $A_0 = A_1 + A_2$. Hence

$$\frac{\partial t}{\partial v_f} = \frac{2r_0 v_\infty^2}{(v_\infty^2 - v_f^2)^2} \frac{A_2}{A_0}. \quad (20)$$

Equation (20) is inserted into the expression for $\epsilon(E^*)$ (Eq. 17) which may then be integrated numerically. This was done for the integration limits $0 \leq v_f \leq 0.99v_\infty$. For $0.99v_\infty < v_f \leq v_\infty$ we assume that no error is made in the transformations, and we therefore add to the integral the fraction of neutrons emitted when $v_f > 0.99v_\infty$, i.e., $\exp[-t(0.99v_\infty)/\tau_n]$. The function $\epsilon(E^*)$ was evaluated for the set of parameters $a = 16.7 \text{ MeV}^{-1}$, $B_n = 7 \text{ MeV}$ and the set $a = 9.7 \text{ MeV}^{-1}$, $B_n = 5 \text{ MeV}$. The fact that the excitation energy E^* decreases for the successive neutrons was taken into account in the following way: The function $\epsilon(E^*)$ was evaluated for a number of excitation energies which correspond (on the average) to the emission of an integral number of neutrons. [These excitation energies were obtained by a Monte Carlo calculation which used the same values a and B_n that were used in the calculation of $\epsilon(E^*)$]. The results for the two sets of parameters are shown in curves (b) and (d) of Fig. 13. Curves (a) and (c) were obtained by summing the values of ϵ [curves (b) and (d)] for integral values of neutron numbers from 1 to n and dividing by n . Thus curves (a) and (c) represent the average error for n neutrons emitted. However, since curves (b) and (d) give this error for the *first* neutron emitted as a function of the excitation energy (translated into number of neutrons), it follows that curves (a) and (c) represent an overestimate of the error (underestimate of ϵ). [A correct calculation of $\epsilon(E^*)$ for the n th neutron should not only take into account that the initial excitation energy was reduced by the emission of the $(n-1)$ previous

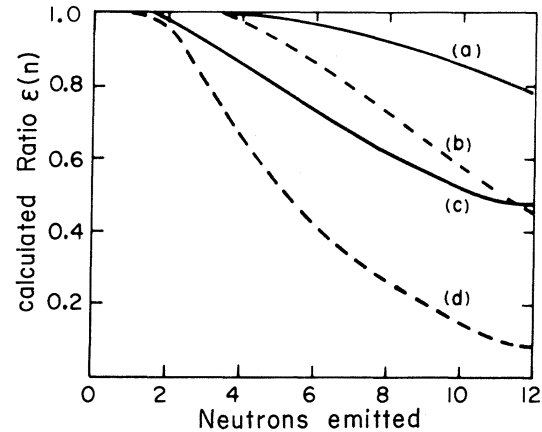


FIG. 13. The ratio of the number of neutrons calculated to be emitted assuming neutron emission occurs only after the fragments have been fully accelerated to the number of neutrons actually emitted, as a function of the number of neutrons emitted per fragment. Curves (b) and (d) show this ratio for the first of n neutrons to be emitted, i.e. the expression $\epsilon(E^*)$ (Eq. 16) as a function of the excitation energy which corresponds to the emission of n neutrons. Curves (a) and (c) show this ratio when averaged over the n neutrons. Curves (a) and (b) were calculated using $a = 16.7 \text{ MeV}^{-1}$ and $B_n = 7 \text{ MeV}$. Curves (c) and (d) using $a = 9.7 \text{ MeV}^{-1}$ and $B_n = 5 \text{ MeV}$. The curves were calculated for symmetric fission of ^{234}U and total fragment kinetic energy of $E_K = 167 \text{ MeV}$.

neutrons, but also the fact that the fragments were already accelerated during the emission of the previous neutrons, i.e., the lower limit of integration for v_f should be >0 .] The curves of Fig. 13 were calculated for symmetric fission of ^{234}U and total fission fragment kinetic energy $E_K = 167 \text{ MeV}$.

In trying to assess, on the basis of Fig. 13, the error in our analysis due to emission of neutrons while the fragments still have not reached their final velocity, note should be taken of two points: (1) Assuming $a = A/10 \text{ MeV}^{-1}$ to be the correct value for the level density parameter, curves (a) and (c) span the fragment mass range $A = 100-160$, with curve (a) appropriate for the heaviest fragment and curve (c) the correct one for fragment mass $A = 100$. The values for fragment masses between these limits fall between the two curves. (2) The average number of neutrons increases rapidly with the fragment mass (Fig. 9); $\bar{\nu} \approx 2$ for $A = 100$ and $\bar{\nu} \approx 6$ for $A = 160$. From Fig. 13, we find that for both cases $\epsilon(n) > 0.95$. We conclude that we analyze correctly the neutron spectrum for 95% of the emitted neutrons.

3. Anisotropic Neutron Emission

(a) *Prefission neutrons.* It has already been stated that the determination of the number of *post*-fission neutrons is not affected by any anisotropy

of the prefission neutrons, since the prefission neutron distribution is isotropic in the detector plane, i.e., a plane perpendicular to the beam direction. Our value for the total number of prefission neutrons will, on the other hand, be affected by the forward-backward peaking of the prefission neutron distribution. This anisotropy results from both the linear and angular momentum transfer to the target nucleus by the bombarding particle. For full momentum transfer (i.e., compound-nucleus formation) in the bombardment of U and Bi by 155-MeV protons, the average angular momentum of the compound nucleus is comparable to that of the compound nucleus formed by the bombardment of Au by 42-MeV α particles. The angular distribution of the neutrons emitted in the latter case is almost isotropic.²⁹ The question of the forward peaking of the prefission neutrons due to linear momentum transfer is more difficult. We have restricted our definition of prefission neutrons to neutrons evaporated after the termination of the prompt cascade. According to the statistical model these neutrons are emitted isotropically in the c.m. system of the excited nucleus, except for possible forward-backward peaking due to the angular momentum effects which we have already discussed. We therefore conclude that within our definition, and assuming the statistical model to correctly describe the evaporation process, our value for the total number of prefission neutrons is correct. However, in nature there is of course no clear separation between the neutrons emitted in the prompt cascade and evaporation neutrons. Harp, Miller, and Berne²³ calculated the number of neutrons evaporated in a highly (1000-MeV) excited nucleus before thermal equilibrium is established and found that only 5% of the particles are emitted before the system of nucleons in the excited nucleus relaxes to an equilibrium energy distribution. There remains however, the question of whether the rapid equilibration of energy among the nucleons in the excited nucleus is accompanied by an equally rapid equilibration of linear momentum. If this is correct, then the results of Harp, Miller, and Berne would indeed mean that 95% of the neutrons are emitted isotropically in the c.m. system of the excited nucleus. This question is not dealt with in the work of Harp, Miller, and Berne. On the other hand, Brun *et al.*³⁰ found that when Au is bombarded with 156-MeV protons, there exists a considerable forward peaking in the emitted neutron distribution, even below kinetic energies of 9 MeV. However, it may in principle be argued that these forward-peaked neutrons do still belong to the prompt nucleon cascade and should not be classified as prefission evaporation neutrons. We conclude that the prefission evapor-

ation neutrons are not well defined, and our experimental method which measures the isotropic part of the prefission neutron distribution represents one way of defining this quantity. There remains the question of whether the prompt-cascade calculations do correctly account for the remaining prefission neutrons.

(b) *Postfission neutrons.* Any possible anisotropy of the postfission neutron in the c.m. system of the fission fragments can only be the result of the angular momentum of the fragment. Three types of experiments show that it is not negligible. From the relatively high yield of fission fragments with isomeric states, Sarantites, Gordon, and Coryell,³¹ concluded that the average angular momentum of the fragments in the thermal-neutron fission of ²³⁵U is $5.5\hbar$, and it is $7.0\hbar$ for ²³⁸U bombarded with 33-MeV α particles. Hoffman³² has measured the angular distribution of the γ rays emitted in thermal-neutron fission of ²³³U and ²³⁵U and concluded that the fragments have an angular momentum of $(7 \pm 2)\hbar$ normal to their direction of motion. Finally, Thomas and Grover³³ fitted the results of an evaporation calculation, which included γ competition, to the number of γ rays emitted in the spontaneous fission of ²⁵²Cf and to the average energy of these γ rays. They obtained good agreement for an average angular momentum of the fragments of $5.5\hbar$.

Angular momentum of the fragments in the plane normal to their direction of motion causes forward-backward peaking of the neutron angular distribution in this direction and thus to an overestimate of the number of postfission neutrons. In order to estimate the size of this effect we again refer to the work of Drake, Axel, and Halpern,²⁹ who measured the angular and energy distributions of the neutrons emitted when aluminium, cobalt, niobium, and gold targets are bombarded with 42-MeV α particles. Of the four targets, niobium is closest to the mass range of the fission fragments. Drake, Axel, and Halpern find that for the niobium target the anisotropy b of the neutron angular distribution, when fitted to the form $W(\theta_{c.m.}) = 1 + b \cos^2 \theta_{c.m.}$ is of the order of $b = 0.1$. (They also find forward peaking of the angular distribution of the high-energy neutrons due to direct interactions, however this effect will not be present in the case of fission fragments.) In view of the much lower average angular momentum of the fission fragments (5.5 – $7\hbar$ as compared to $\sim 15\hbar$ in the case of a niobium target bombarded with 42-MeV α particles), the anisotropy of the angular distribution of the postfission neutrons in the c.m. system of the fragment will be substantially smaller than 10%. Indeed, when Milton and Fraser²⁶ tried to fit the postfission neutron distribution in the thermal-

neutron fission of ^{235}U to the form $W(\theta_{\text{c.m.}}) = 1 + b \cos^2 \theta_{\text{c.m.}}$, they found that the best fit was obtained for $b = 0$, i.e., isotropic evaporation. We conclude that the angular momentum of the fragment will not affect our results within the experimental errors.

B. Ratio of the Number of Neutrons at 0 and 90° with Respect to the Fission Fragment Direction (U Target)

The $N(0^\circ)/N(90^\circ)$ ratio is related to the number of pre-fission and post-fission neutrons. The experimental results of $N(0^\circ)/N(90^\circ)$ for neutrons with lab energy between 0.5 and 9.0 MeV are 2.05–2.45 for U and 1.77–2.11 for Bi. (These numbers have not been corrected for the finite solid angle of the detectors.) The lower and upper limits refer to the two efficiency curves which are used to analyze the 90° data. The statistical errors are only ± 0.1 for each target. The results for U disagree with the ratio $N(0^\circ)/N(90^\circ)$ reported by Harding and Farley¹ in 1956. They obtained $N(0^\circ)/N(90^\circ) = 1.27 \pm 0.11$ for neutrons emitted in the fission of ^{238}U induced by 145-MeV protons. They detected the neutrons with the aid of methane proportional counters, and their lower limit of detection was a neutron kinetic energy of 1.8 MeV as compared to 0.5 MeV in our experiment. The disagreement between the two results is even larger if we consider only neutrons above 1.8 MeV in our experiment.

Based on their experimental results, Harding and Farley concluded that of the 13 neutrons emitted in the reaction (this number was determined in a separate experiment by Harding²), only 2.5 ± 1 are post-fission neutrons. Their conclusions were based on the comparison of the experimental $N(0^\circ)/N(90^\circ)$ ratio with the results obtained from an evaporation calculation.

We have also performed calculations in order to obtain the $N(0^\circ)/N(90^\circ)$ ratio which is predicted by the conventional model of the prompt cascade followed by fission-spallation competition. The calculation of the prompt intranuclear cascade for ^{238}U bombarded with 155-MeV protons was carried out in the manner described by Chen *et al.*¹⁴ This calculation yields the distribution (A, Z, E^*) of the excited nuclei at the end of the fast cascade. This information was used as an input for a calculation of the fission-spallation competition. This calculation followed, in general, the method of Dostrovsky *et al.*^{34,35} The following assumptions were made in the calculation:

(1) The pre-fission neutrons are emitted isotropically in the lab system and the post-fission neutrons are emitted isotropically in the c.m. system of the fully accelerated fragments.

(2) The fragment kinetic energy, mass, and charge divisions are Gaussian distributions with the experimental mean values and standard deviations, and with $Z_1/Z_2 = A_1/A_2$. No mass-kinetic-energy correlation was assumed.

(3) The total excitation energy of the fission fragments is equal to $(E^* + \Delta M - E_K)$, where E^* is the excitation energy of the nucleus prior to fission, ΔM is the mass difference between the fissioning nucleus and the two fragments,²⁰ and E_K is the total kinetic energy of the fission fragments. The excitation energy of the fragments is divided between the fragments in proportion to their masses. (The experimental results show that more neutrons are emitted from the heavy fragments than would be predicted by this relation.) This effect tends to lower somewhat the experimental $N(0^\circ)/N(90^\circ)$ ratio, since more neutrons are correlated with the slower moving heavy fragments.

(4) The level-density parameter is $a_n = 25 \text{ MeV}^{-1}$ before fission and $a_n = A/7 \text{ MeV}^{-1}$ for neutron emission from the fission fragments. Lower values of a_n for neutron emission from the fragments (e.g., $a_n = A/10 \text{ MeV}^{-1}$) result in an increase in $N(0^\circ)/N(90^\circ)$ since the kinetic energy of the neutrons in the c.m. system of the fragments is increased.

The calculations were performed for three different assumptions with respect to the ratio Γ_f/Γ_n of fission width to neutron-emission width.

(1) Γ_f/Γ_n is independent of the excitation energy E^* and dependent only on the (A, Z) of the excited nucleus. The actual values of Γ_f/Γ_n were taken from Vandenbosch and Huizenga.³⁶

(2) Γ_f/Γ_n as given by the statistical model.^{34,22}

$$\frac{\Gamma_f}{\Gamma_n} = \frac{K_0 a_n \{2[a_f(E^* - E_f)]^{1/2} - 1\}}{4 A^{2/3} a_f(E^* - B_n)} \times \exp \{2[a_f(E^* - E_f)]^{1/2} - 2[a_n(E - B_n)]^{1/2}\}, \quad (21)$$

where E_f is the height of the fission barrier and a_f is the level-density parameter at the fission barrier. The other symbols have the same meaning as in Eq. (12). The values of E_f were obtained from the empirical relation of Vandenbosch and Seaborg.³⁷ We assume $a_f = a_n = 25 \text{ MeV}^{-1}$.

(3) $\Gamma_f = 0$ for $E^* > 10 \text{ MeV}$, $\Gamma_f = \infty$ for $E^* \leq 10 \text{ MeV}$. The purpose of this assumption was to obtain the lowest possible $N(0^\circ)/N(90^\circ)$ ratio by forcing fission to occur only at the very last step of the evaporation cascade.

The results of our calculations for these three assumptions are shown in Table IV. The calculated values for $N(0^\circ)/N(90^\circ)$ have been corrected for the finite solid angles of the detectors in our

TABLE IV. The calculated number of prefission and postfission neutrons and $N(0^\circ)/N(90^\circ)$ for $^{238}\text{U} + 155\text{-MeV } p$ for three formulations of Γ_f/Γ_n . Also shown are the experimental values. All numbers pertain to the neutron lab energy range 0.5–9.0 MeV.

Energy dependence of Γ_f/Γ_n	Number of prefission neutrons	Number of postfission neutrons	$N(0^\circ)/N(90^\circ)$
(1) Γ_f/Γ_n – independent of E^*	1.1	10.5	2.90
(2) Γ_f/Γ_n as given by statistical model	5.8	6.2	2.36
(3) $\Gamma_f = 0$ $E^* > 10$ MeV $\Gamma_f = \infty$ $E^* \leq 10$ MeV	9.5	2.34	1.70
Experimental	5.7 ± 1.0	5.2 ± 0.5	2.05–2.45

experiment. They pertain to the neutron lab energy range 0.5–9.0 MeV.

Table IV shows that the calculated values based on the first assumption (Γ_f/Γ_n independent of excitation energy) do not agree with the experimental results. Neither does the third assumption (fission at $E^* < 10$ MeV) give results compatible with the experimental values. The latter was to be expected. However, the results of the third assumption show that even with the most extreme value for Γ_f/Γ_n , we are unable to reproduce the experimental value of Harding and Farley¹ for $N(0^\circ)/N(90^\circ)$, despite the fact that they made a calculation with similar assumptions and obtained agreement with their experimental value $N(0^\circ)/N(90^\circ) = 1.27 \pm 0.11$.

The calculated values based on the second assumption [Γ_f/Γ_n given by Eq. (21)] are in good agreement with our experimental result (except for a slight discrepancy for the number of postfission neutrons). Yet when the same calculation is made for Bi bombarded with 155-MeV protons (also assuming $a_n = a_f$), the calculation predicts that fission should not occur at all. LeBeyec and Lefort⁷ have shown that with the same equation for Γ_f/Γ_n good agreement can be obtained for the spallation residues of Bi + 156-MeV p if low values for the fission barriers of the neutron-deficient isotopes of Po and Bi are used.³⁸ This is further discussed in the next section. A restricted conclusion which may be drawn from Table IV, and which is quite independent of the particular expression used for Γ_f/Γ_n , is that the calculations confirm that a $N(0^\circ)/N(90^\circ)$ ratio of 2.0–2.5 corresponds to an approximately equal number of prefission and postfission neutrons.

C. Comparison with Radiochemical Results and Measurements of Fission Cross Sections

Information on the competition between fission and neutron emission in the deexcitation of excited heavy nuclei can also be obtained from the measurement of total fission cross sections and the yield of spallation residues in high-energy reac-

tions in heavy nuclei. Indeed any calculation of such reactions must correctly predict not only the number of prefission and postfission neutrons, but also the total fission cross section and the cross sections for the formation of the residual nuclei which have not undergone fission. Conversely, a meaningful comparison between the three types of experimental results can only be made through a theoretical calculation of the reaction. The three types of experimental results may be said to agree with each other if a given theoretical model correctly predicts all of them.

Lindner and Osborne measured the spallation yields for ^{238}U and ^{232}Th bombarded with protons of energy 100–340 MeV.⁴ These results were later analyzed by Lindner and Turkevich.³ They calculated the spallation yields assuming the usual sequence of a fast intranuclear cascade followed by neutron evaporation and fission. They obtained good agreement with the experimental results assuming Γ_f/Γ_n to be energy independent (our assumption 1). Using the energy-dependent expression of Eq. (21), they obtained calculated cross sections for the isotopes ^{232}U and ^{228}U of 29 and 4.4 mb, respectively, whereas the experimental values were 3 and 0.03 mb, respectively. Similar disagreement was obtained when fission was restricted to low excitation energies only (similar to our third assumption). However, our calculation and the calculation of Lindner and Turkevich used somewhat different models for the fast intranuclear cascade process, and the fission-neutron-emission competition calculation of Lindner and Turkevich used approximations which were not made in our calculation. Therefore, it is not certain that our results and the results of Lindner and Osborne disagree with each other.

LeBeyec and Lefort⁷ have studied the radiochemical yields of the residual nuclei in the bombardment of ^{209}Bi by 156-MeV protons. They obtained agreement between calculations based on the prompt cascade followed by fission–neutron-emission competition and their experimental results, when low values for the fission barrier of

the neutron-deficient isotopes were used in Eq. (21).³⁸ The effect of using low fission barriers in the calculation is that fission occurs towards the end of the neutron-evaporation process. Such an effect can also be obtained if a_f/a_n is not constant but is assumed to be higher at low excitation energies. Khodai-Joopari³⁹ has shown that at excitation energies below 35 MeV, best agreement is obtained between the calculated fission cross sections and the experimental values for α -particle and proton bombardments of Bi and lead for $a_f/a_n = 1.35-1.45$. At higher excitation energies such a ratio predicts fission cross sections which are ten times larger than the experimental values.

We have performed calculations similar to those which we made for uranium for the reaction $^{209}\text{Bi} + 155\text{-MeV } p$. Equation (21) was used for Γ_f/Γ_n , and the values for E_f were obtained from the work of Khodai-Joopari.³⁹ A wide range of values was tried for the level-density parameters a_f and a_n (assumed to be energy independent). Within these limitations on E_f , a_f , and a_n , we were unable to obtain a set of parameters which would give good agreement with all three types of experimental results, namely the number of pre-fission and postfission neutrons, the cross sections for the spallation residues, and the fission cross sections.

Thus we tentatively conclude that the classical model of prompt cascade followed by fission-neutron-evaporation competition, with Γ_f/Γ_n as given by the statistical model (Eq. 21) and with the usual assumptions for E_f , a_f , and a_n , is unable to predict both the number of pre-fission and postfission neutrons as obtained in this experiment for ^{209}Bi and ^{238}U and the radiochemical results with the same set of parameters. It seems that in order to obtain better agreement, at least in the case of Bi, Γ_f/Γ_n must be assumed to decrease with increasing excitation energy. Both the low fission barriers which Le Beyec, Lefort, and Peter³⁸ found necessary to use, and the very high ratio for a_f/a_n which Khodai-Joopari³⁹ found to give the best fit at low excitation energies seem to support this view. Moreover Thompson, Moretto, and Gatti⁴⁰ find that in α -particle bombardments of tungsten isotopes, the function Γ_f/Γ_n flattens or even decreases above excitation energies of 60-70 MeV despite the fact that Eq. (21) would predict Γ_f/Γ_n to increase rapidly with energy.

We expect on quite general grounds the statistical model formulation for Γ_f/Γ_n to become invalid at high excitation energies. In this formulation no cognizance is taken of the fact that the transition of the nucleus to the saddle point involves the collective motion of the whole nucleus,

whereas the equivalent transition in the case of neutron emission consists of scattering a single nucleon into an unbound state. In particular the transition-state method [which is the theoretical basis for Γ_f in Eq. (21)] assumes statistical equilibrium between all states of the system, be they single-particle excitations of the nucleus in its ground-state deformation, or levels associated with the nucleus at the saddle-point deformation. This assumption breaks down when the time associated with the transition from the ground-state deformation to the saddle-point deformation is of the same order of magnitude or larger than the total lifetime of the excited system. We thus expect that at high excitation energies Γ_f/Γ_n will be lower than the value obtained from Eq. (21).

A more definite statement on the agreement between the various experimental results and between these results and any particular energy dependence of Γ_f/Γ_n must await a more detailed analysis of both the calculations and the various experimental results.

D. Division of the Excitation Energy between the Two Fragments

The number of neutrons emitted from a given fragment is to a first approximation proportional to the excitation energy of the fragment. From the average slope of the total fission fragment kinetic energy *versus* the number of neutrons (Fig. 12), we obtain for the factor of proportionality 8.8 MeV/neutron for Bi and 7.6 MeV/neutron for U. Figure 9 shows that the average number of neutrons emitted from a fragment increases strongly with the fragment mass. The slope of $\bar{\nu}(A_f)$ at the most probable mass value (symmetric fission) is 0.051 neutrons/amu for Bi and 0.055 neutrons/amu for U. We thus find that the slope of the excitation energy *versus* fragment mass is 0.45 MeV/amu for Bi and 0.42 MeV/amu for U (for the most probable mass value).

The statistical model predicts that if the two fragments are in "thermal equilibrium" up to the moment of scission, the excitation energy of the two fission fragments should be proportional to their mass (equal nuclear "temperature") except for that part of the fragment excitation energy which had its origin in the deformation energy of the fragments at the moment of scission. Disregarding the deformation energy we would expect, therefore, the slope to be approximately equal to $\bar{\nu}/A_0$ ($\bar{\nu}$ is the average number of postfission neutrons, and A_0 is the mass number of the fissioning nucleus), i.e., 0.021 neutrons/amu for Bi and 0.022 neutrons/amu for U. The mass dependence of the deformation energy as obtained

from the calculations of Nix and Swiatecki⁴¹ on the two-spheroid approximation to the liquid-drop model for Bi is even smaller than the above values (~ 0.15 MeV/amu, see Fig. 23 of Ref. 41).

Plasil, Ferguson, and Schmitt (PFS)⁴² also concluded from their work that the slope of $\bar{\nu}(A_f)$ is much steeper than predicted by the two-spheroid approximation of the liquid-drop model. They bombarded ^{209}Bi with 53.25-MeV α particles and obtained $\bar{\nu}(A_f)$ by indirect neutron counting. Their curve $\bar{\nu}(A_f)$ has a somewhat higher slope than ours. This may be explained by the mass dispersion in our results due to the prompt intranuclear cascade which results in a distribution of excited nuclei. The effect of this mass dispersion is a decrease in the slope of $\bar{\nu}(A_f)$. No such mass dispersion exists in the experiment of PFS. However, PFS obtain for the average number of neutrons $\bar{\nu} = 7.4 \pm 1.0$, whereas we obtain $\bar{\nu} = 4.2 \pm 0.5$ for $^{209}\text{Bi} + 155\text{-MeV } p$. PFS indicate that their value for $\bar{\nu}$ might be slightly too large. Yet there seems to remain a serious discrepancy between these two results.

In order to clarify the disagreement with the results of the liquid-drop-model calculations for $d\bar{\nu}/dA_f$, we write the total excitation energy E_i^* of the fragment at the moment of scission as the sum of the deformation energy X_i and the "internal" energy E_i^{int} ,

$$E_i^* = X_i + E_i^{\text{int}} = X_i + a_i T^2,$$

where T is the nuclear temperature of the fissioning nucleus, and $a_i = cA_i$ is the nuclear-level-density parameter. Differentiating, we obtain

$$\frac{\partial \nu_i}{\partial A_f} = \frac{1}{\bar{E}_n} \frac{\partial E_i^*}{\partial A_f} = \frac{1}{\bar{E}_n} \left(\frac{\partial X_i}{\partial A_f} + cT^2 \right), \quad (22)$$

where \bar{E}_n is the average energy required for the emission of one neutron. The calculations of Nix⁴¹ show the function $\partial X_i/\partial A_f$ to be a rapidly varying function of the fissility parameter x in the region of Bi ($x \approx 0.70$), and hence the value of $\partial X_i/\partial A_f$ is very sensitively dependent on the choice of $(Z^2/A)_{\text{crit}}$. (See Fig. 23 of Ref. 41). Moreover, it should be stressed that the calculations of Nix were made for a two-spheroid approximation of the liquid-drop model, and that a more accurate calculation may well yield a higher value of $\partial X_i/\partial A_f$.

The liquid-drop calculations of Nix and Swiatecki are not valid for U. However, for this nucleus there exist low-energy data with which we can compare our results. It has been noted by Cheifetz and Fraenkel¹⁸ and by Burnett *et al.*⁴³ who measured $\bar{\nu}(A_f)$ for the reaction $^{238}\text{U} + 12\text{-MeV } p$ and for $^{233}\text{U} + (8.5\text{--}13.0)\text{ MeV } p$, respectively, that the main effect of the increase in excitation energy of

the compound nucleus on $\bar{\nu}(A_f)$ is an increase in the number of neutrons emitted from the *heavy* fragment, whereas little increase is noted in the number of neutrons from the light fragment. The same effect is observed when we compare our results for $^{238}\text{U} + 155\text{-MeV } p$ to the results for intermediate excitation energies.^{18,43} The sudden drop in the "staircase" curve of $\bar{\nu}(A_f)$ for the heavy fragment is almost completely "filled in" at high excitation energies, whereas little increase is noted in $\bar{\nu}(A_f)$ for the light fragments. Thus the additional excitation energy of the fissioning system seems to be almost exclusively concentrated in the heavy fragment, whereas the increase in the excitation energy of the light fragment is relatively small. This result does not necessarily indicate that statistical equilibrium prior to scission is not maintained. It most probably means that the nuclear equation of state is more complicated than the relation $E^* = aT^2$ with $a = cA$. At low excitation energies the level-density parameter a for nuclei far from closed shells is indeed roughly proportional to the mass number, but is smaller for closed shell nuclei. As the excitation energy increases, the level-density parameter for mid-shell nuclei remains constant but it increases for closed-shell nuclei. Hence the relative amount of excitation of the closed-shell nuclei will increase as the excitation energy increases. A second factor which is also associated with the disappearance of the shell effects at higher energies is the decrease of the stiffness to deformation of closed-shell nuclei at higher energies. These nuclei therefore also acquire a larger share of the *deformation* energy at higher excitation energies.

VI. SUMMARY

In our experiment we measured the angular and energy distribution of the neutrons as a function of the total kinetic energy of the fission fragments and of the mass division in fission induced by 155-MeV protons on ^{209}Bi and ^{238}U . Based essentially on only one assumption, namely: The postfission neutrons are emitted isotropically in the c.m. system of the fully accelerated fragments, we obtained the number of postfission neutrons as a function of the fragment mass. The number of prefission neutrons was obtained on the basis of an additional assumption: The prefission neutrons are emitted isotropically in the lab system. Our results are: 5.8 ± 1.0 prefission neutrons and 5.1 ± 0.5 postfission neutrons in the case of U, and 6.9 ± 1.0 prefission neutrons and 4.2 ± 0.5 postfission neutrons in the case of Bi. The results have been corrected for neutrons with velocities outside the experimental upper and lower limits of detec-

tion. The possible errors in the number of post-fission neutrons due to neutron emission before the fragments attained their final velocity and due to the anisotropy of emission in the c.m. system of the fragment are within our stated experimental error.

Isotropic emission in the lab system of the pre-fission neutrons might be regarded as an operational definition of the pre-fission neutrons, rather than an assumption. Such a definition is necessary since the prompt-cascade and evaporation processes cannot be clearly separated, either experimentally or theoretically. Therefore there exists no sharp distinction between the prompt cascade and the pre-fission evaporation neutrons. An additional source of ambiguity is the neutrons which are emitted between the moment the nucleus reaches the saddle point and the moment of scission. From the theoretical point of view these neutrons should probably be regarded as postfission neutrons, but experimentally they are indistinguishable from the pre-fission neutrons.

Calculations based on the usual model of a fast intranuclear cascade followed by neutron-evaporation-fission competition were carried out. The level-density parameters and fission barrier used in these calculations were taken from low-energy data. We were unable to obtain a consistent set of parameters which would fit the pre-fission and postfission neutron data, the radiochemical cross sections for the spallation residues, and the experimentally measured fission cross sections. It seems that better agreement would obtain if the fission probability (Γ_f/Γ_n) is assumed to decrease at higher excitation energies.

The average number of postfission neutrons as a function of fragment mass was found to increase strongly with increasing fragment mass for both Bi and U. In the case of Bi these results are in disagreement with the predictions of the liquid-drop model. Comparing our results for U with the results at lower excitation energies, we find that almost all the additional excitation energy is concentrated in the heavy fragment.

ACKNOWLEDGMENT

Two of the authors (E.C. and Z. F.) wish to thank Professor M. Lefort and the Institut de Physique Nucléaire for their hospitality during the experiments. Two of us (J. P. and E. C.) are grateful to the French Centre National de la Recherche Scientifique and the National Research Council of Israel for their financial support. The authors wish to thank Dr. J. R. Nix for his valuable comments regarding this work.

APPENDIX A. EFFECT OF THE RECOIL MOMENTUM ON THE FRAGMENT DETECTION EFFICIENCY

In the following we try to evaluate the experimental bias in our results due to the deviation from collinearity of the two fission fragments in the lab system. This deviation affects the detection efficiency of the two fission fragments.

The deviation of the fragments from collinearity in the lab system is due to three factors:

- (1) The linear momentum imparted to the target nucleus by the bombarding particle.
- (2) The recoil of the excited nucleus due to the emission of pre-fission neutrons.
- (3) The recoil of the fragment due to the emission of postfission neutrons.

In addition, the detection efficiency of the two fission fragments is reduced as a result of the finite size of the bombarding beam. (In our experiment the beam size was much smaller than the size of the target.)

The effect of the deviation from collinearity and finite beam size on the detection efficiency of the two fragments was reduced in our experiment by using two detectors of different active areas (3 and 4 cm²). However this was not sufficient to achieve the ideal situation: that, if one fragment is detected by the smaller detector, its partner is invariably detected by the larger detector.

In the evaluation of the effect of the deviation from collinearity, we shall utilize the experimental work of Stephan and Perlman¹⁰ who measured the deviation from collinearity of the fragments in the fission of U, Bi, and Ta induced by 155-MeV protons. In their experiment they fixed one fragment detector at 90° to the beam and measured both the in-plane (polar) and out-of-plane (azimuthal) angular distributions of the second fragment with respect to the direction of the first one. Their results show that for the U target, the in-plane angular distribution peaks at a forward angle of 4° (with respect to the center line of the second detector, normal to the beam) and has a FWHM of 10°, whereas the out-of-plane angular distribution has a FWHM (at the in-plane forward angle of 4°) of 7°. For Bi the in-plane distribution peaks at a forward angle of 7° and has a FWHM of 7°. The out-of-plane distribution was not measured for Bi. The average forward deflection angle is the result of the momentum imparted to the target nucleus by the bombarding particle during the fast intranuclear-cascade process. The latter process, as well as neutron evaporation, are responsible for distribution of the in-plane and out-of-plane angles around the average deflection angle. Stephan and Perlman also calculated for U the fast

intranuclear-cascade process using a Monte Carlo method,⁴⁴ and presented their results in the form of the distribution of the excited nuclei as a function of their forward momentum P_{\parallel} and their excitation energy E^* at the end of the fast-cascade process. Their calculation gave good agreement with their experimental results. The results of these calculations will be used here in order to estimate the efficiency of detecting both fission fragments in our experiment as a function of the excitation energy E^* prior to the neutron-evaporation process. Since the number of neutrons emitted in the evaporation cascade is roughly linearly related to the initial excitation energy, we thus obtain the detection efficiency as a function of the number of emitted neutrons.

The experimental arrangement is shown in schematic form in Fig. 14(a). The beam is in the z direction. The large detector of radius r_2 is placed along the x axis at a distance d from the target. The smaller detector of radius r_1 is placed in the x - z plane at a forward angle θ with respect to the x axis and at the same distance from the target. θ was set equal to the average deflection angle as determined by Stephan and Perlman,¹⁰ i.e., 4° for U and 7° for Bi. The detector and target projections in the y - z plane are shown in a schematic way in Fig. 14(b). Since θ is small, the projection of detector 1 may be approximated by a circle. For a collinear fission event which originated at a point (y_1, z_1) on the target and in

which one of the fragments hit detector 1, there exists a circular disk of radius r_1 and center $(2y_1, 2z_1 + \theta d)$ in the plane of detector 2 within which the second fragment will hit. The ratio of overlapping area between this disk and the area of detector 2 [shaded area in Fig. 14(b)] to the area of detector 1 represents the detection efficiency of our system.

The detection efficiency of the two fragments as a function of the deviation $\Delta\theta$ of their recoil angle from the angle θ of the experimental arrangement was calculated by integrating numerically the coincidence efficiency for all points of the effective target area (actually the beam cross section).

The results of the calculation for our experimental conditions are shown in Fig. 15 for both a point source in the center of the target and the actual effective target area of 0.5-cm radius. Although the absolute efficiency is higher for a point source, the variation of the efficiency as a function of the deviation angle $\Delta\theta$ is smaller for a finite target area.

The detection efficiency of the fragment pair as a function of the excitation energy E^* of the nucleus at the beginning of the neutron-evaporation cascade is shown in Fig. 16. The figure was obtained by integrating numerically the results of Stephan and Perlman for the average excitation energy E^* as a function of the forward momentum P_{\parallel} with the results of Fig. 15. The relation between p_{\parallel} and the recoil angle θ of the fragments is given by

$$\theta = (p_{\parallel}/p_f)(A_f/A_0),$$

here p_{\parallel} is the recoil momentum of the excited nucleus in the beam direction, p_f is the fragment momentum in the c.m. system of the fissioning nucleus (\approx lab momentum of the fragment), A_f is the

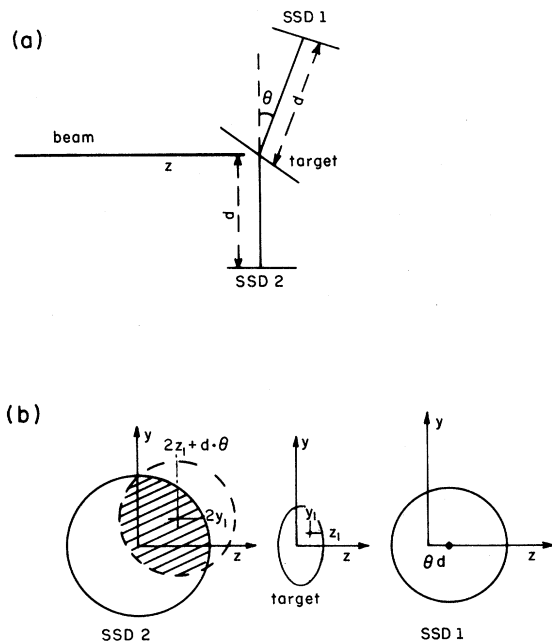


FIG. 14 (a), (b) The experimental arrangement of the target and fission fragment detectors in schematic form.

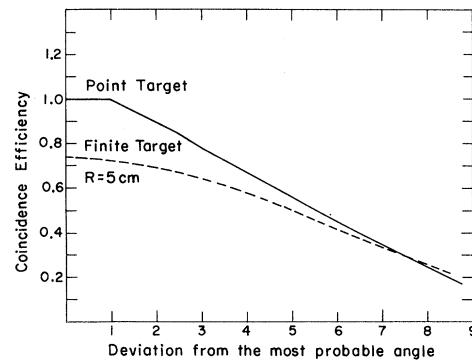


FIG. 15. Fission-fragment-coincidence detection efficiency as a function of the deviation $\Delta\theta$ from the most probable recoil angle for a point target and a target of radius $R = 0.5$ cm.

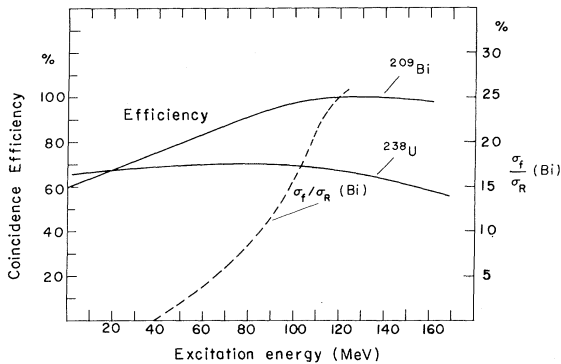


FIG. 16. Fission-fragment-coincidence detection efficiency for Bi and U as a function of the excitation energy E^* of the excited nucleus prior to the neutron-evaporation cascade. Also shown is Γ_f/Γ_R (ratio of fission cross section to the total reaction cross section) as a function of E^* for Bi.

fragment mass, and A_0 is the mass of the fissioning nucleus (\approx target nucleus). We see that in the extreme cases of (a) compound-nucleus formation (p_{\parallel} equal to the momentum of the incoming particle), and (b) the formation of an excited nucleus with the minimum energy required for fission (6 MeV), the detection efficiency changes by less than 10% from its maximum value (mean recoil momentum).

The situation is somewhat different in the case of Bi, since here the mean recoil momentum p_{\parallel} in the beam direction for those nuclei which subsequently undergo fission is above the average value for all cascades, and the mean excitation energy of these nuclei at the beginning of the evaporation cascade is above the average value for all cascades. This may also be restated in the following way: Whereas in the case of U the fission probability is roughly independent of the initial excitation energy, and hence the average excitation energy E^* for nuclei undergoing fission is close to the average excitation energy of *all* nuclei at the beginning of the evaporation cascade, this is not so for Bi. In this case mainly nuclei with excitation energy E^* above the average value will eventually undergo fission. Therefore the mean recoil angle (and hence the deflection angle θ of detector 1) in the case of Bi is close to the maximum value, and the detector efficiency for small recoil angles (low excitation energy E^*) is substantially lower than the maximum value. This is seen in Fig. 16. Since Stephan and Perlman did not calculate the average excitation energy as a function of recoil momentum p_{\parallel} for Bi, we obtained the Bi curve by calculating $E^*(p_{\parallel})$ with the Monte Carlo program of Chen *et al.*¹⁴ One may conclude on the basis of Fig. 16 that our measurements had a large experi-

mental bias in the case of Bi. This however is not so. Stephan and Perlman found that the FWHM of the recoil-angle distribution for Bi was 7° (as compared to 10° for U), and since the mean recoil angle is 7° fission events with small recoil angles are very infrequent. This is the result of the very small fission cross section at low excitation energies for nuclei in the Bi region. In order to illustrate this point, we also show in Fig. 16 the ratio σ_f/σ_R for the reaction $\text{Pb}^{206} + \text{He}^4$ as obtained by Khodai-Joopari.³⁹ (σ_f is the fission cross section, σ_R is the total reaction cross section.)

So far we have dealt only with the effect of the parallel component p_{\parallel} of the recoil momentum. The distribution of the transverse component p_{\perp} of the recoil momentum may be obtained from the distribution of out-of-plane recoil angles. As already mentioned, Stephan and Perlman measured this distribution and found a FWHM of 7° in the case of U (the mean out-of-plane angle is, of course, zero). One may reasonably assume that a similar number holds for Bi. Since this width is equal to or smaller than the width of the in-plane recoil-angle distribution, the effect of the p_{\perp} distribution on the detection efficiency will be similar or somewhat smaller than the effect of the p_{\parallel} distribution which was discussed above. However, whereas there exists a definite correlation between p_{\parallel} and E^* , essentially no correlation exists between E^* and the transverse component of the recoil momentum due to the fast cascade.¹⁴ This is not true for the transverse recoil momentum due to neutron evaporation. However, altogether, the correlation between p_{\perp} and E^* is much weaker than that between p_{\parallel} and E^* .

Finally we must consider the bias introduced in our measurement because of the (triple coincidence) requirement of detecting a neutron in addition to the two fission fragments. This neutron causes a deviation from collinearity because of the recoil momentum which it imparts to the fragment. The effect of this recoil momentum on the fragment detection efficiency is entirely negligible for neutrons detected at 0° to the fragment (it would be strictly zero if not for the finite acceptance angle of the neutron and fragment detectors). The effect is larger for neutrons emitted at 90° to the fragments. Here the detection efficiency is diminished as a result of the recoil momentum imparted by the neutron, and it is a function of the neutron velocity (the effect is largest for the neutrons of highest energy). Unlike the effects of the finite distributions of p_{\parallel} and p_{\perp} on the detection efficiency discussed above, we can readily correct for the effect of the triple coincidence requirement by explicitly calculating the fragment detection efficiency as a function of the neutron velocity,

and correcting the results accordingly. Such corrections were indeed made in the experiments of Milton and Fraser⁴⁵ and Bowman *et al.*⁸ However the acceptance angle of their detection systems was very much smaller than ours. A neutron emitted at 90° with a lab energy of 9 MeV will result for the average U fission fragment in a deflection angle of 1.8°. This recoil angle reduces the detection efficiency by only 5% (see Fig. 15). Neutrons of lab energy of 9 MeV at 90° to the fragments are very rare indeed, and the reduction in efficiency because of the recoil of most neutrons is entirely negligible. We therefore did not correct our data for this effect.

To summarize, the largest bias to the fragment detection efficiency is caused by the parallel component p_{\parallel} of the recoil momentum imparted to the target nucleus by the bombarding particle. This bias results in a reduction of less than 10% in the detection efficiency over the whole range of possible excitation energies for U. The effect is larger for Bi at low excitation energies, but the probability of fission at these energies is very small. Thus the effect of the recoil momentum imparted to the target nucleus and to the fission fragments by the incoming particle and by the evaporated neutrons is well within our experimental errors.

APPENDIX B. CALCULATION OF THE FRAGMENT ENERGY AND MASS

The fragment energy is first approximated by the relation

$$E'_i = cX_i + d,$$

where X_i is the pulse height (channel number) of fragment i , $c = 24.4/(P_L - P_H)$ MeV, and $d = (79.4 - cP_H)$ MeV. P_L and P_H are the pulse heights of the light and heavy peaks, respectively, for the ²⁵²Cf fission energy spectrum.

The next step is to correct for energy losses in the target, backing, and the protection foils in front of the detectors. We used the relation given by Alexander and Gazdick⁴⁶

$$\Delta E_i = C(E'_i + \overline{\Delta E})^{1/3} W, \quad (23)$$

where ΔE_i is the energy loss of fragment i , C is a constant which depends on the stopping material, W is the thickness of the stopping material, and $\overline{\Delta E}$ is the average energy loss of the median fragment. The first approximation for the fragment masses is

$$A'_1 = A_0 E_2'' / (E_1'' + E_2''), \quad A_2 = A_0 - A'_1, \quad (24)$$

where $E_i'' = E'_i + \Delta E_i$, and A_0 is the mass of the

fissioning nucleus (we assume $A_0 = 234$ for U and $A_0 = 205$ for Bi). Based on A'_1 , A'_2 , X_1 , and X_2 , the energies E_1 and E_2 are recalculated using Eq. (1) (see Sec. III), and E_i and A_i are recalculated using Eqs. (23) and (24). The energies E_1 and E_2 are the fragment energies after neutron emission. The initial (preneutron emission) kinetic energy is approximated by

$$\tilde{E}_i = E_i (1 + \bar{\nu}(A_i, E_K) / A_i), \quad (25)$$

where $\bar{\nu}(A_i, E_K)$ is the average number of neutrons emitted by fragment A_i when the total kinetic energy of the two fragments is E_K . We assume

$$\bar{\nu}(A_i, E_K) = \bar{\nu}(A_i) + [E_K - \bar{E}_K(A_i)] \frac{\partial \bar{\nu} / \partial E_K}{\bar{E}_K}. \quad (26)$$

$\bar{\nu}(A)$ is the average number of neutrons from fragment A_i , $\bar{E}_K(A_i)$ is the average total kinetic energy for the mass division A_i and $(A_0 - A_i)$, and $\frac{\partial \bar{\nu} / \partial E_K}{\bar{E}_K}$ is the weighted average of the variation of the number of neutrons as a function of E_K . $\bar{\nu}(A_i)$, $\bar{E}_K(A_i)$, and $\frac{\partial \bar{\nu} / \partial E_K}{\bar{E}_K}$ were measured in the present experiment. Both Eqs. (25) and (26) involve the approximation of taking the average values $\bar{\nu}(A_i, E_K)$ and $\frac{\partial \bar{\nu} / \partial E_K}{\bar{E}_K}$ instead of the true values (which were not measured). In addition we assume in Eq. (26) that $\bar{\nu}(A_i, E_K) \approx \bar{\nu}(A_i, \tilde{E}_K)$. (\sim designates preneutron emission quantities.)

Once the preneutron emission energies \tilde{E}_1 and \tilde{E}_2 are determined, we obtain the initial mass values as in Eq. (24)

$$\tilde{A}_1 = A_0 \tilde{E}_2 / (\tilde{E}_1 + \tilde{E}_2), \quad \tilde{A}_2 = A_0 - \tilde{A}_1. \quad (27)$$

The experimental uncertainties in the determination of the total kinetic energy and the fragment mass are the results of the following factors:

(1) The energy resolutions of the solid-state detectors. According to Schmitt, Kiker, and Williams¹³ this resolution is approximately 1.5 MeV FWHM or $\sigma^2 = 0.4$ MeV².

(2) The uncertainty in the number of neutrons emitted from a fragment of mass A_i , i.e., the variance of the function $\bar{\nu}(A_i)$. This variance has not been measured so far for any fissioning system. We therefore estimate this variance to be $\sigma^2(\nu) = \bar{\nu}$. For the median fragment in our experiment $\bar{\nu} = 2.5$ neutrons/fragment. This yields a kinetic-energy uncertainty of variance $\sigma^2(E_i) = 1.8$ MeV² for both U and Bi.

(3) The effective target thickness, W (in MeV), for the median fragment was 5.6 MeV for U and 2.0 MeV for Bi. Since the energy-loss distribution is rectangular, its variance is given by $\frac{1}{12} W^2$ which is 2.6 MeV² for U and 1.25 MeV² for Bi.

(4) The channel width was approximately 1.2 MeV/channel resulting in a variance (Sheppard's correction) of 0.12 MeV².

The total variance in the measurement of the single-fragment kinetic energy was thus 4.9 MeV^2 for U and 3.6 MeV^2 for Bi.

The target thickness does not contribute significantly to the error in the measurement of the total kinetic energy of the two fragments, since the total energy loss of the two fragments is essentially constant. The uncertainty due to straggling is much lower than the other errors which are discussed here. Thus the variance of the total kinetic energy $E_K = E_1 + E_2$ is given by $2 \times (0.4 + 1.8 + 0.1) = 4.6 \text{ MeV}^2$, or $\sigma = 2.15 \text{ MeV}$, for both Bi and U.

The uncertainty in the determination of the fragment masses is obtained from Eq. (24) which yields

$$(\delta A_1/A_1)^2 = (\delta E_2/E_2)^2 + (\delta E_K/E_K)^2 \quad (28)$$

and a similar equation for $(\delta A_2/A_2)$. The uncertainty in δE_K in Eq. (28) includes only errors in measuring E_1 , since the errors in E_2 are already included in δE_2 . The total uncertainty in the determination of the fragment masses has a standard deviation of $\sigma_A = 3.3 \text{ amu}$ for U and 2.9 amu for Bi. However, these values are based on the assumption of a unique fissioning mass A_0 ($A_0 = 234$ for U and $A_0 = 205$ for Bi). As already mentioned, one has a distribution of fissioning nuclei, and the width of these distributions for Bi and U increases the uncertainty in the determination of the absolute fragment masses. It does not affect the mass ratio.

APPENDIX C. EFFECTS OF NEUTRON SCATTERING ON THE NEUTRON-DETECTION EFFICIENCY

The neutron detection efficiency was obtained by the comparison of the experimental energy distribution of the neutrons emitted in the spontaneous fission of ^{252}Cf with the results of Bowman *et al.*⁸ In the following, we shall discuss the effect of neutron scattering inside the chamber and, in particular, in the chamber walls on our experimental neutron energy distribution. Neutrons which are scattered from objects outside the vacuum chamber towards the neutron detectors may be neglected since their flight time will be above the limit of the time-to-amplitude converters. On the other hand, γ rays from $(n, n'\gamma)$ reactions may be detected by our system.

Neutron scattering inside the chamber and in the chamber walls affects the measured neutron energy spectrum in two ways: (a) It changes the velocity spectrum of the detected neutrons; (b) it changes the measured angular distribution of the neutrons. The effect on the energy distribution is to shift the spectrum to *lower* energies, since the flight path of the scattered neutrons is lengthened

and their velocity lowered. The γ rays from $(n, n'\gamma)$ reactions cause, on the other hand, a shift to *higher* energies, since they simulate high-energy neutrons.

As a result of neutron scattering, the measured angular distribution of the neutrons is more isotropic than the original distribution, since more neutrons are scattered out of the direction of the peak of the distribution (0°) into the direction of the minimum (90°) than vice versa. The γ rays of the $(n, n'\gamma)$ reactions have a similar effect on the angular distribution. As a result of the increase in the measured distribution at 90° compared to the distribution at 0° , the effective detection efficiency at 90° as determined by our method, is higher than that at 0° .

The $N(0^\circ)/N(90^\circ)$ ratio for the ^{209}Bi and ^{238}U targets in our experiment was much smaller than that for ^{252}Cf [$N(0^\circ)/N(90^\circ) \approx 7$ for ^{252}Cf]. This means that the relative effect of neutron scattering for Bi and U was larger at 0° and smaller at 90° than for ^{252}Cf . Thus the neutron detection efficiency for Bi and U at *all* angles was larger than the ^{252}Cf 0° efficiency and smaller than the ^{252}Cf 90° efficiency. In other words, the efficiency curves for 0 and 90° which were obtained on the basis of the Cf measurements are upper and lower limits of the true efficiency for all angles of the Bi and U measurements. However, since the neutron spectrum and the effect of scattering for Bi and U at 0° are very similar to those of Cf at 0° , we used the 0° Cf efficiency curves for the Bi and U measurements at 0° . For the 90° Bi and U measurements the 0° Cf efficiency curve is also the better approximation, and it was therefore used for the 90° data as well. However the numbers in Table III are the average values of the results obtained on the basis of the 0 and 90° Cf efficiency curves.

We mentioned above that scattered neutrons which reach the detectors add to the neutron spectrum at lower energies, whereas the γ rays from $(n, n'\gamma)$ reactions add to it at higher energies. However, since the neutron spectrum falls off rapidly with increasing energy, the relative effect of the scattered neutrons is much smaller than that of the γ rays. This was shown in Fig. 4, where the experimental efficiencies at 0° for the two detectors are compared with the calculated efficiency. The theoretical curve was calculated assuming a single scattering in the plastic scintillator (52.5% H, 47.5% C). Scattering inside the chamber and in the chamber walls was not taken into account in this calculation. It is seen that for high neutron velocities the experimental curves are substantially higher than the calculated one, indicating the sizable effect of γ rays from $(n, n'\gamma)$

reactions, and possibly insufficient separation of the high-energy neutrons and the prompt γ peak of the time-of-flight spectrum. The higher detection threshold of PM II decreased not only the efficiency for low-energy neutrons (low energy end of efficiency curve), but also decreased the efficiency of detecting low-energy γ rays. Therefore the efficiency of PM II is also lower at the high-velocity end of the spectrum.

We have also tried to calculate the contribution of neutron scattering in the chamber walls to the measured neutron distribution for the spontaneous fission of ^{252}Cf . The chamber was assumed to consist of a spherical aluminium shell of 30-cm radius and 0.7-cm thickness. The experimental spectra of Bowman *et al.*⁸ were used as input data. Elastic and inelastic scattering of neutrons as well as γ rays from $(n, n'\gamma)$ reactions were considered. The elastic scattering data were taken from Emmerich,⁴⁷ whereas the inelastic scattering cross section was assumed to be isotropic. The probability of exciting the various excited states of ^{27}Al was taken from the Nuclear Data Sheets.⁴⁸ The calculated direct and scattered "neutron" spectra at 0 and 90° with respect to the fission fragment direction are shown in Fig. 17. It is seen that at 0° the effect of the scattered neutrons and photons is negligible except for the lowest neutron velocities, whereas this effect is much more important at 90°, particularly at the low and high ends of the neutron velocity spectrum. As already mentioned, the 90° neutron spectrum for Cf is of little relevance for our experimental results.

The conclusion that the scattering corrections for the 0° spectrum are negligible except for neutron velocities below ~ 1.5 cm/nsec is not verified by the comparison of the experimental efficiency at 0° with the calculated curve with no scattering correction (Fig. 4). This comparison shows good agreement for low-velocity neutrons and substantial deviations above ~ 3 cm/nsec. Since the calculated curves of Fig. 4 and Fig. 17 are of approximate nature, the reason for the discrepancy is not obvious. It may be that most of the deviation at high energies is due to insufficient separation of the high-energy neutrons and the γ peak in the time-of-flight spectrum.

APPENDIX D. CALCULATION OF THE NUMBER OF POSTFISSION NEUTRONS

The total number $n_{ij}(\theta)$ of neutrons at an angle θ and in the velocity interval j in a given mass-energy box i is given by

$$n_{ij}(\theta) = \frac{NC_{ij}(\theta) \times 4\pi}{\epsilon_j(\theta) R \omega Y_i}, \quad (28)$$

where $NC_{ij}(\theta)$ is the number of neutron counts in the velocity interval j and mass-energy box i at angle θ , $\epsilon_j(\theta)$ is the effective neutron detection efficiency for neutron velocity v_j at angle θ , R is the total number of fission coincidences (uncorrelated with neutrons) which were measured in the experiment, Y_i is the relative fission yield for the mass-energy box i , ω is the solid angle of the neutron detector.

The general expression for the postfission neu-

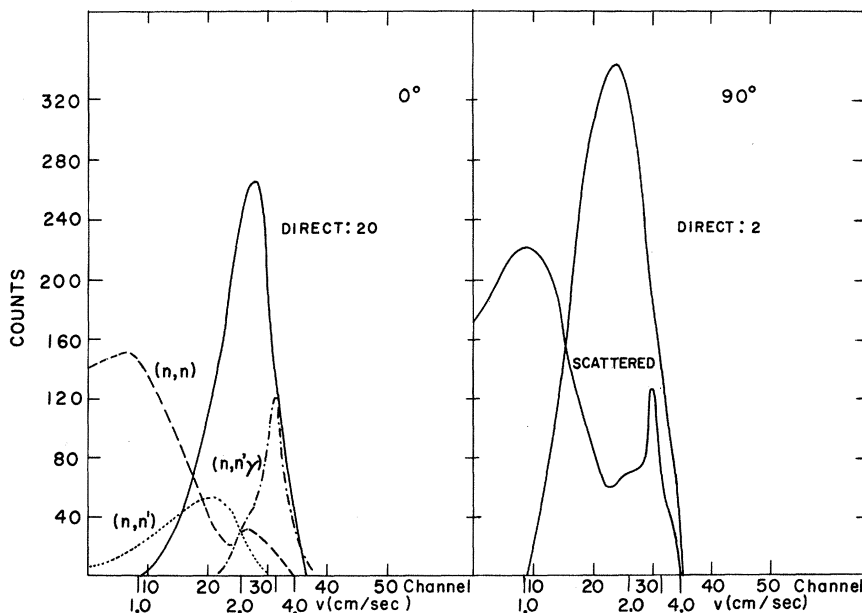


FIG. 17. The contribution of elastically and inelastically scattered neutrons and photons from $(n, n'\gamma)$ reactions to the measured neutron time-of-flight spectrum for the spontaneous fission of ^{252}Cf at 0 and 90° with respect to the fission fragment direction. The three components are shown separately for the 0° spectrum and jointly for the 90° spectrum.

tron spectrum $N_i(\text{c.m.})$ for mass-energy box i after one iteration is given by Eq. (10):

$$N_i(\text{c.m.}) = D^{(0)}N_i(\text{c.m.}) + D^{(1)}N_i(\text{c.m.}) + D^{(2)}N_i(\text{c.m.}).$$

The explicit form for the upper-limit assumption (first assumption) of the neutron spectrum in mass-energy box i , fragment 1 is given by the expression

$$\begin{aligned} N_i(\text{c.m.}) = & T_i(0, \text{c.m.}, 1)[N_i(0) - N_i(90)] \\ & + T_i(0, \text{c.m.}, 1)T_i(\text{c.m.}, 90, 1)T_i(0, \text{c.m.}, 1)N_i(0) \\ & + T_i(0, \text{c.m.}, 1)T_i(\text{c.m.}, 90, 2)T_i(180, \text{c.m.}, 2)N_i(180) \\ & - T_i(0, \text{c.m.}, 1)T_i(\text{c.m.}, 0, 2)T_i(180, \text{c.m.}, 2)N_i(180). \end{aligned} \quad (29)$$

For the lower-limit assumption (second assumption) we obtain

$$\begin{aligned} N_i(\text{c.m.}) = & T_i(0, \text{c.m.}, 1)[N_i(0) - N_i(90)] \\ & + T_i(0, \text{c.m.}, 1)T(\text{c.m.}, 90, 1)T_i(0, \text{c.m.}, 1)[N_i(0) - N_i(90)] \\ & + T_i(0, \text{c.m.}, 1)T_i(\text{c.m.}, 90, 2)T_i(180, \text{c.m.}, 2)[N_i(180) - N_i(90)] \\ & - T_i(0, \text{c.m.}, 1)T_i(\text{c.m.}, 0, 2)T_i(180, \text{c.m.}, 2)[N_i(180) - N_i(90)]. \end{aligned} \quad (30)$$

$N_i(\theta)$ is the neutron spectrum for mass-energy box i at angle θ . The transformation operators T_i are given by:

$$T_i(\theta, \text{c.m.}, k) = v_{\text{c.m.}}(v_L - v_{ik} \cos \theta)/v_L^2, \quad (31a)$$

$$T_i(\text{c.m.}, \theta, k) = v_L^2/[v_{\text{c.m.}}(v_L - v_{ik} \cos \theta)]. \quad (31b)$$

$v_{\text{c.m.}}$ and v_L are the neutron c.m. and lab velocities, respectively, and v_{ik} is the velocity of fragment k associated with mass-energy box i , θ is the angle with respect to fragment 1. The transformations are not commutative. We see that the upper- and lower-limit expressions (Eqs. 29 and 30) differ from each other in the operand of the second to fourth terms.

APPENDIX E. EVALUATION OF THE NUMBER OF NEUTRONS WITH KINETIC ENERGIES ABOVE OR BELOW THE EXPERIMENTAL DETECTION LIMITS

We wish to estimate the number of neutrons which were not detected in our measurements because their lab energy was below the lower limit of detection (0.5 MeV) or above the upper detection limit (9.0 MeV). Prefission neutrons are almost solely affected by the lower detection limit, whereas the postfission neutron spectrum is only sensitive to the upper detection limit. The upper limit of detection in terms of the c.m. energy of the postfission neutrons has an average value of 5.2 MeV (3.2 cm/nsec). In the following, we shall be mainly concerned with the number of the postfission neutrons above the upper detection limit.

The calculation for the number of prefission neutrons below the lower detection limit follows the same lines. We make the following assumptions:

(1) The c.m. kinetic energy spectrum of the neutrons has a Maxwellian form

$$n(\epsilon)d\epsilon = (\epsilon/T^2)e^{-\epsilon/T}d\epsilon, \quad (32)$$

where ϵ is the neutron energy, and T is the nuclear temperature of the fragment. T is related to the excitation energy E^* in the usual manner, $E^* = aT^2$. We assume $a = 14 \text{ MeV}^{-1}$.

(2) The *initial* excitation energy distribution of the fission fragments prior to neutron emission is rectangular between the limits E_{min} and E_{max} . E_{min} is the lowest excitation energy at which neutron emission is possible.

(3) The evaporation of a neutron reduces the excitation energy of the fragment by a constant amount.

It follows from assumption (2) and (3) that the excitation energy distribution of all fragments along the evaporation cascade has a triangular form

$$P(E^*)dE^* = 2[(E_{\text{max}} - E^*)/(E_{\text{max}} - E_{\text{min}})^2]dE^*. \quad (33)$$

The spectrum of all neutrons emitted in the evaporation cascade is given by

$$\begin{aligned} N(\epsilon)d\epsilon = & \int_{E_{\text{min}}}^{E_{\text{max}}} P(E^*)[\epsilon/T(E^*)^2] e^{-\epsilon/T(E^*)} \\ & \times \frac{\partial T}{\partial E^*} dE^* d\epsilon. \end{aligned} \quad (34)$$

The number of neutrons above the detection limit ϵ_{\max} is

$$I(\epsilon_{\max}) = \int_{\epsilon_{\max}}^{E_{\max}} \int_{E_{\min}}^{E_{\max}} P(E^*) [\epsilon/T(E^*)^2] \times e^{-\epsilon/T(E^*)} \frac{\partial T}{\partial E^*} dE^* d\epsilon. \quad (35)$$

The integral $I(\epsilon_{\max})$ can be evaluated analytically if the upper limit of integration with respect to ϵ is changed from E_{\max} to infinity. This change introduces a negligible error. The number of neutrons above $v_{\max} = (2\epsilon_{\max}/m)^{1/2}$ is shown in Fig. 18 for various values of E_{\max} - the upper limit of the fragment excitation energy distribution. The lower limit of the excitation energy distribution was assumed to be $E_{\min} = 5$ MeV.

The upper velocity detection limit for the post-fission neutrons is $v_{\max} = (4.3 - v_f)$ cm/nsec in the c.m. system, v_f is the fragment velocity. For an upper limit of the fragment excitation energy distribution $E_{\max} = 45$ MeV and a fragment velocity of $v_f = 1.1$ cm/nsec, about 10% of the postfission neutrons are above our detection limits. This is true for both U and Bi.

The correction for the average number of post-fission neutrons as a function of the fragment mass A_f (Fig. 9) was made by evaluating the mean velocity v_f of fragment A_f from the experimental data and the mean initial excitation energy $\bar{E}^* = \frac{1}{2}(E_{\max} + E_{\min})$ of the fragment from the average number of neutrons $\bar{\nu}(A_f)$. Both \bar{E}^* and v_{\max} increase with the fragment mass A_f . As a result, the percentage $I(v_{\max})$ of undetected neutrons is a rather slowly varying function of A_f . It increases from 8% for the lightest fragments to 13% for the heaviest fragments.

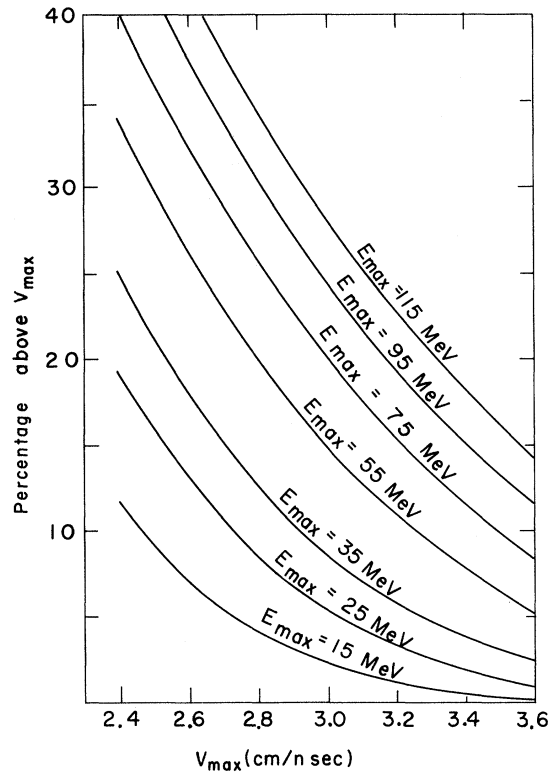


FIG. 18. The percentage of neutrons above the c.m. velocity v_{\max} as a function of v_{\max} for various values of the highest excitation energy E_{\max} of the fragment.

The number of prefission neutrons below the lower detection limit is given by an integral identical to Eq. (25) except that the limits of integration are between 0 and 0.5 MeV. The result is that approximately 7% of the prefission neutrons are not detected in our experiment.

¹G. N. Harding and F. J. M. Farley, Proc. Phys. Soc. (London) **A69**, 853 (1956).

²G. N. Harding, Proc. Phys. Soc. (London) **A69**, 330 (1956).

³M. Lindner and A. Turkevich, Phys. Rev. **119**, 1632 (1960).

⁴M. Lindner and R. N. Osborne, Phys. Rev. **103**, 378 (1956).

⁵M. Lefort, G. N. Simonoff, and X. Tarrago, Nucl. Phys. **25**, 216 (1961).

⁶B. D. Pate and A. M. Poskanzer, Phys. Rev. **123**, 647 (1961).

⁷Y. Le Beyec and M. Lefort, Nucl. Phys. **A99**, 131 (1967).

⁸H. R. Bowman, S. G. Thompson, J. C. D. Milton, and W. J. Swiatecki, Phys. Rev. **126**, 2120 (1962).

⁹L. Kowalski and C. J. Stephan, J. Phys. (Paris) **24**, 901 (1963).

¹⁰C. J. Stephan and M. L. Perlman, Phys. Rev. **164**, 1528 (1967).

¹¹Manufactured by Nuclear Enterprises Ltd., Edinburgh 11, Scotland.

¹²M. Gettner and W. Selove, Rev. Sci. Inst. **31**, 450 (1960).

¹³H. W. Schmitt, W. E. Kiker, and C. W. Williams, Phys. Rev. **137**, B837 (1965).

¹⁴K. Chen, Z. Fraenkel, G. Friedlander, J. R. Grover, J. M. Miller, and Y. Shimamoto, Phys. Rev. **166**, 949 (1968).

¹⁵J. Terrell, Phys. Rev. **127**, 880 (1962).

¹⁶J. S. Fraser, in *Proceedings on the Symposium on Physics and Chemistry of Fission, Salzburg, Austria, 1965* (IAEA Vienna, Austria, 1965), Vol. I, p. 451.

¹⁷K. Skarsvåg and K. Bergheim, Nucl. Phys. **45**, 72 (1963).

¹⁸E. Cheifetz and Z. Fraenkel, Phys. Rev. Letters **21**,

36 (1968).

¹⁹J. Galin, M. Lefort, J. Peter, X. Tarrago, E. Cheifetz, and Z. Fraenkel, Nucl. Phys. **A134**, 513 (1969).

²⁰W. D. Myers and W. J. Swiatecki, University of California Lawrence Radiation Laboratory, Report No. UCRL 11980, 1965 (unpublished).

²¹J. R. Nix, Ann. Phys. **41**, 52 (1967); J. R. Nix, Nucl. Phys. **A130**, 241 (1969).

²²J. R. Huizenga and R. Vandenbosch, in *Nuclear Reactions*, edited by P. M. Endt and P. B. Smith (North Holland Publishing Co., Amsterdam, The Netherlands, 1962), Vol. II.

²³G. D. Harp, J. M. Miller, and B. J. Berne, Phys. Rev. **165**, 1166 (1968).

²⁴J. M. Miller, private communication. We thank Professor Miller for performing this calculation for us.

²⁵Y. Boneh, Z. Fraenkel, and I. Nebenzahl, Phys. Rev. **156**, 1305 (1967).

²⁶J. C. D. Milton and J. C. Fraser, in *Proceedings of the Symposium on the Physics and Chemistry of Fission, Salzburg, Austria, 1965* (IAEA, Vienna, Austria, 1965), Vol. II, p. 39.

²⁷W. D. Loveland, A. W. Fairhall, and I. Halpern, Phys. Rev. **163**, 1315 (1967).

²⁸V. P. Eismont, Atomnaya Energi. **19**, 113 (1965) [transl.: Soviet J. At. Energy **19**, 1000 (1965)].

²⁹D. M. Drake, P. Axel, and I. Halpern, in *Proceedings of the Conference on Direct Interactions and Nuclear Reaction Mechanisms, Padua, Italy, 1962*, edited by E. Clementel and C. Villi (Gordon and Breach Publishers, Inc., New York, 1963).

³⁰C. Brun, H. Dubost, G. Gatty, M. Lefort, and X. Tarrago, Nucl. Phys. **A295**, 337 (1967).

³¹D. G. Sarantites, G. E. Gordon, and C. D. Coryell, Phys. Rev. **138**, B353 (1965).

³²M. M. Hoffman, Phys. Rev. **133**, 714 (1964).

³³T. D. Thomas and J. R. Grover, Phys. Rev. **159**, 980 (1967).

³⁴I. Dostrovsky, Z. Fraenkel, and P. Rabinovitch, in

Proceedings of the Second United Nations International Conference on the Peaceful Uses of Atomic Energy, Geneva, Switzerland, 1958 (United Nations, Geneva, Switzerland, 1958), Vol. 15, p. 301.

³⁵I. Dostrovsky, Z. Fraenkel, and G. Friedlander, Phys. Rev. **116**, 683 (1959).

³⁶R. Vandenbosch and J. R. Huizenga, in *Proceedings of the Second United Nations International Conference on the Peaceful Uses of Atomic Energy, Geneva, Switzerland, 1958* (United Nations, Geneva, Switzerland, 1958), Vol. 15, p. 284.

³⁷R. Vandenbosch and G. T. Seaborg, Phys. Rev. **110**, 507 (1958).

³⁸Y. LeBeyec, M. Lefort, and J. Peter, Nucl. Phys. **88**, 215 (1966).

³⁹A. Khodai-Joopari, University of California Lawrence Radiation Laboratory Report No. UCRL 16489, 1966 (unpublished).

⁴⁰S. G. Thompson, L. Moretto, and R. Gatti, private communication.

⁴¹J. R. Nix and W. J. Swiatecki, Nucl. Phys. **71**, 1 (1965).

⁴²F. Plasil, R. L. Ferguson, and H. W. Schmitt, in *Proceedings of the Second Symposium on the Physics and Chemistry of Fission, Vienna, Austria, 1969* (IAEA, Vienna, Austria, 1969), p. 505.

⁴³S. C. Burnett, R. L. Ferguson, F. Plasil, and H. W. Schmitt, Phys. Rev. Letters **21**, 1350 (1968).

⁴⁴J. P. Cohn, Nucl. Phys. **84**, 316 (1966).

⁴⁵J. C. D. Milton and J. S. Fraser, Phys. Rev. **111**, 877 (1958).

⁴⁶J. M. Alexander and M. F. Gazdik, Phys. Rev. **120**, 874 (1960).

⁴⁷W. S. Emmerich, in *Fast Neutron Physics*, edited by J. B. Marion and J. L. Fowler (Interscience Publishers, Inc., New York, 1963), Vol. II, p. 1057.

⁴⁸*Nuclear Data Sheets*, compiled by K. Way *et al.* (Printing and Publishing Office, National Academy of Sciences-National Research Council, Washington, D.C.).